catalysts

MDPI

Review

Insights into Photo/Electrocatalysts for the Degradation of Per- and Polyfluoroalkyl Substances (PFAS) by Advanced Oxidation Processes

Xiaoyan Chen [1,2,*], Taoyue Yuan [1], Xinyu Yang [1], Shunke Ding [3] and Mengtao Ma [1,*]

[1] Department of Chemistry and Materials Science, College of Science, Nanjing Forestry University, 159 Longpan Road, Nanjing 210037, China
[2] State Key Laboratory of Pollution Control and Resource Reuse, School of the Environment, Nanjing University, Nanjing 210023, China
[3] College of Environment, Hohai University, 1 Xikang Road, Nanjing 210098, China
* Correspondence: sheris_chen@njfu.edu.cn (X.C.); mengtao@njfu.edu.cn (M.M.)

Abstract: Per- and polyfluoroalkyl substances (PFASs) are an emerging group of persistent organic pollutants in aquatic environments with high levels of toxicity and bioaccumulation. The risks posed by PFASs to the environment and health have attracted increasing attention. To remove them from water, advanced oxidation processes (AOPs), with the merits of high efficiency and low cost, are mainly used. Photo/electrocatalytic heterogeneous AOPs, with the assistance of nanostructured catalysts and external energy in the form of light/electricity, have emerged as one of the most powerful techniques, overcoming the difficulty associated with defluorination and achieving the effective and complete degradation of PFASs in water. The structures of photo/electrocatalysts play a critical role in the production of reactive oxygen species, the electron transfer process, and the degradation pathway and its efficiency. Herein, to elucidate the structure–performance relationship, a review of photo/electrocatalysts for the enhanced degradation of PFASs in heterogeneous AOPs, organized according to their composition and nanostructure design, is provided. This review article is mainly focused on (1) the mechanisms and pathways of PFAS degradation by heterogeneous photo/electrocatalytic AOPs, and (2) the structural designs and modifications of photo/electrocatalysts for the enhanced degradation of PFASs by heterogeneous AOPs. Finally, the challenges and prospects for future research into photo/electrocatalysts of heterogeneous AOPs in the field of PFAS remediation are discussed.

Keywords: per- and polyfluoroalkyl substances (PFASs); heterogeneous advanced oxidation processes (AOPs); photo/electrocatalytic degradation; photocatalysts; electrocatalysts

Citation: Chen, X.; Yuan, T.; Yang, X.; Ding, S.; Ma, M. Insights into Photo/Electrocatalysts for the Degradation of Per- and Polyfluoroalkyl Substances (PFAS) by Advanced Oxidation Processes. *Catalysts* **2023**, *13*, 1308. https://doi.org/10.3390/catal13091308

Academic Editors: Tahir Muhmood and Xiaofei Yang

Received: 28 August 2023
Revised: 13 September 2023
Accepted: 15 September 2023
Published: 19 September 2023

1. Introduction

Per- and polyfluoroalkyl substances (PFASs) are an emerging group of persistent organic pollutants in the environment which pose ecological and health risks [1]. PFASs are man-made chemicals that are widely used in various industrial and commercial products; their chemical structure includes a fully fluorinated carbon chain with a terminated functional group attached to it. The most common terminal groups are carboxylic acid (−COOH) and sulfonic acid ($-SO_3H$) groups, while the fluorinated carbon chain varies in length and number of branches, containing a number of carbon–fluorine bonds. Perfluorooctanoic acid (PFOA) and perfluorooctane sulfonate (PFOS), with structural formulas shown in Figure 1a, are the two most commonly detected PFASs. The carbon–fluorine bond in these molecules is one of the strongest single bonds due to its bond energy of 485–582 kJ/mol and its redox potential of F/F^- at 3.6 eV, making it difficult for PFASs to break down naturally [2]. Moreover, the fluorine atoms in PFASs provide a shielding effect that protects the carbon–fluorine bond from chemical and biological attack, further

contributing to the persistence of these compounds. On the other hand, toxicological and epidemiological studies have linked PFAS exposure to adverse health effects. For example, the presence of PFOA and PFOS in human blood samples collected worldwide, at a concentration level of μg/L, has been demonstrated to be harmful, causing developmental and reproductive problems, immune system dysfunction, hormonal imbalances, etc. Due to their persistence and potential risks, PFASs are considered a major environmental and public health concern, making them a research focus for scientists, regulators, and policymakers all over the world. The U.S. EPA set a health advisory level of 0.070 μg/L for PFASs in 2016; this level was recently reduced to 0.004 ng/L for PFOA and 0.02 ng/L for PFOS [3]. The EU Water Framework Directive has proposed a limit value of 0.1 μg/L for twenty PFASs in total [4]. In many cases, however, the PFAS levels in drinking water sources surpass the safety threshold, necessitating treatment methodologies for PFASs in water to mitigate their adverse effects.

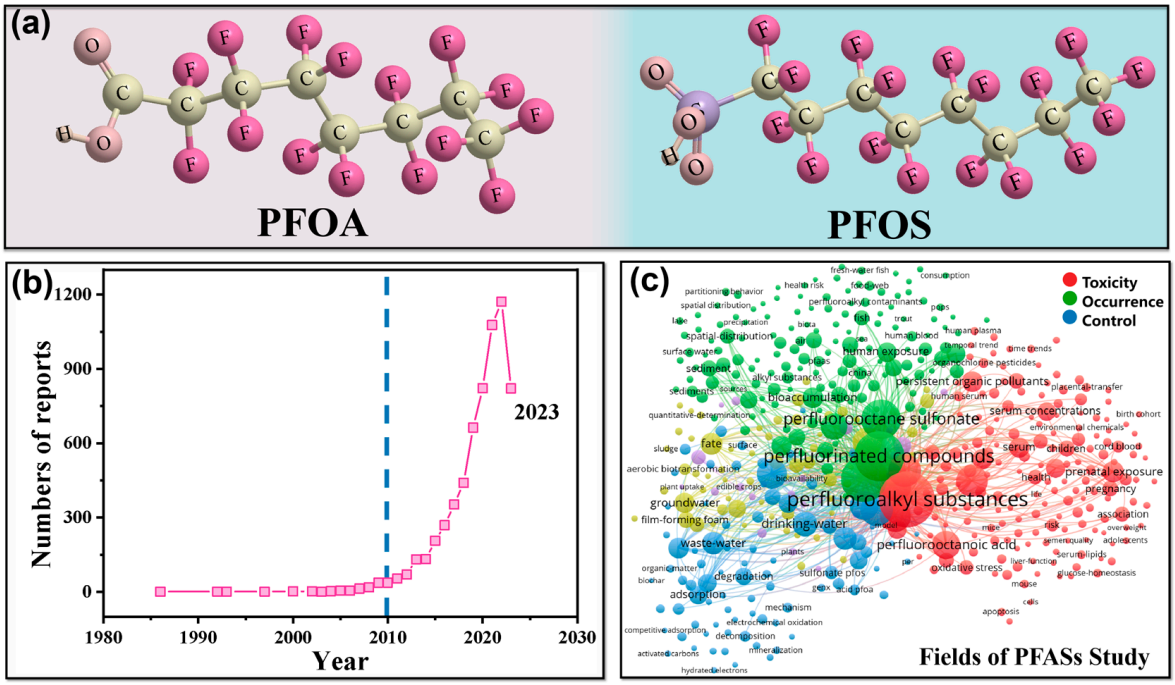

Figure 1. (**a**) The structures of PFOA and PFOS, and the most commonly occurring PFASs in aquatic environments. (**b**) Volume of reported research on PFASs. (**c**) Heat map of works on PFASs, mainly addressing toxicity, occurrence, and control. Data collected from Web of Science (up to 2023).

Recent years have witnessed a boom in studies of PFASs, including strategies for their control in water, as displayed in Figure 1b,c. These strategies can be categorized into three principal types, i.e., physical separation [5,6], biological treatment [7], and chemical degradation (oxidation and reduction processes) [8–11]. Physical removal technologies, including adsorption, ion exchange, reverse osmosis, and nanofiltration, either have low PFAS elimination efficiency or high cost [6]. These non-destructive processes may generate waste such as spent adsorbents that can give rise to re-contamination with their re-entry into the environment. Biological degradation and chemical degradation are destructive technologies that permanently remove PFASs from water, but biodegradations are incomplete, have slow rates, and are highly dependent on environmental conditions [12]. Traditional wet chemical oxidation can barely break the very strong C–F bonds, whereas advanced oxidation processes (AOPs), originally introduced by Glaze in 1987 and distinguished by employing free radicals as highly reactive oxidant species, are considered to be highly efficient and have strong potential for the complete mineralization of PFASs [13,14]. To overcome the high overpotential of defluorination from C–F bonds and accelerate decomposition, more effective AOPs have been developed by introducing catalysts and external

energy (light, electricity, heat, ultrasound, etc.) to lower the activation energy and overpotential of PFAS degradation reactions [15–18]. Energy in the forms of light and electricity is more appropriate for in situ use, as such approaches are relatively low-cost and environmentally friendly. Therefore, photocatalytic and electrocatalytic AOPs in heterogeneous systems are promising for the efficient and complete removal of PFASs in practice. These AOPs have recently attracted considerable research interest, with a vast body of relevant literature [19–28].

Numerous review articles have provided broad overviews of different water treatment methods for PFAS remediation [29–35], among which some have reviewed general AOPs for PFAS degradation [34,35]. In contrast, the present review will focus on heterogeneous photo/electrocatalytic AOPs. This is a group of promising treatment methods with enhanced PFAS mineralization is characterized by the involvement of catalyst materials and optical/electrical energy. Since comprehensive analyses of the similarities and differences of these processes in terms of PFAS degradation are still rare, this review aims to give overall and targeted insights into the photocatalytic and electrocatalytic degradation of PFASs by heterogeneous AOPs, from the fundamental mechanisms to catalyst designs. This review may facilitate further research on developing advanced photocatalysts and electrocatalysts for efficient PFAS removal by AOPs.

2. Fundamentals of PFAS Degradation by AOPs

In comparison with conventional homogeneous AOPs, heterogeneous AOPs for PFAS degradation are improved systems with incorporated catalysts. Heterogeneous AOPs use catalysts to activate oxidating agents (e.g., H_2O_2, O_3, persulfate), which contribute to the generation of powerful reactive oxidant species (ROS) such as hydroxyl radicals (•OH) and sulfate radicals (SO_4^{-}•) [36,37]. Defluorination and the elimination of head groups (e.g., carboxylate and sulfonate groups) are linked, depending on the dominant ROS, contributing to the loss of head groups or breaking C−F bonds in perfluoroalkyl chains [38]. Identifying effective ROS and their transformation pathways during oxidation reactions may provide insights into PFAS degradation mechanisms, which are fundamental for the design of heterogeneous AOPs [39].

2.1. General Pathways and ROS for PFAS Degradation

The degradation by AOPs of PFASs occurring in water environments starts with their hydrolysis products (Equation (1)). Below, perfluorocarboxylic acid (PFCA, $C_nF_{2n+1}COOH$) represents the PFAS, while the effective ROS is represented by •OH. The degradation mechanisms of PFASs by AOPs are closely linked to ROS and their effective sites of action. However, these pathways can be summarized as a general reaction course [40]. Specifically, the oxidation of $C_nF_{2n+1}COO^-$ to $C_nF_{2n+1}COO$• (Equation (2)) is initiated by radicals (e.g., •OH) generated from activated oxidizing agents [41]. Light and electrical energy can also trigger this reaction, utilizing, for example, photogenerated holes (h^+) under ultraviolet radiation or the electron transfer process at the anode [42]. Subsequently, spontaneous decarboxylation of $C_nF_{2n+1}COO$• occurs due to its instability (Equation (3)), and the resulting perfluoralkyl radicals C_nF_{2n+1}• transform into $C_nF_{2n+1}OH$ via hydroxylation (Equation (4)) [43]. After the spontaneous elimination of HF from $C_nF_{2n+1}OH$ (Equation (5)), the resulting acyl halide, $C_{n-1}F_{2n-1}COF$, undergoes a hydrolysis process (Equation (6)), generating a short-chain PFCA ($C_{n-1}F_{2n-1}COO^-$). Afterwards, this decarboxylation-hydroxylation-elimination-hydroxylation (DHEH) procedure is performed repeatedly, with the remove of a CF_2 unit and the release of CO_2 and HF in each cycle (Equations (2)–(6)) until complete mineralization is achieved [44,45]. The general degradation pathways of perfluorosulfonic acid (PFSA) are similar, but with the initial oxidation of $C_nF_{2n+1}SO_3^-$ to C_nF_{2n+1}• by ROS attacking the C−S bond [46]. The resulting product then enters the defluorination cycle, similarly to PFCA.

$$C_nF_{2n+1}COOH \rightarrow C_nF_{2n+1}COO^- + H^+ \quad (1)$$

$$C_nF_{2n+1}COO^- + \bullet OH\left(/ + h^+ / - e^-\right) \rightarrow C_nF_{2n+1}COO\bullet + OH^- \quad (2)$$

$$C_nF_{2n+1}COO\bullet \rightarrow C_nF_{2n+1}\bullet + CO_2 \quad (3)$$

$$C_nF_{2n+1}\bullet + \bullet OH \rightarrow C_nF_{2n+1}OH \quad (4)$$

$$C_nF_{2n+1}OH \rightarrow C_{n-1}F_{2n-1}COF + HF \quad (5)$$

$$C_{n-1}F_{2n-1}COF + H_2O \rightarrow C_{n-1}F_{2n-1}COO^- + HF + H^+ \quad (6)$$

Effective ROS in AOPs of PFASs vary based on the oxidizing agents and their activation methods. Free radicals, such as •OH, sulfate radicals ($SO_4^-\bullet$), and superoxide radicals ($\bullet O_2^-$), as well as nonradicals like singlet oxygen ($^1O_2$) and holes (h^+), have been identified as dominant ROS that contribute individually or synergistically to the defluorination and destruction of PFASs through advanced oxidation [47]. Fenton and Fenton-like processes, using hydrogen peroxide (H_2O_2) as the oxidant, generate •OH as the effective ROS when activated by Fe^{2+} or other transition metal-based chemicals or materials. Activated persulfate systems, utilizing persulfate (PDS, $S_2O_8^{2-}$) or peroxymonosulfate (PMS, HSO_5^-), primarily generate $SO_4^-\bullet$ as the dominant ROS and exhibit reactivity due to the high redox potential (+ 2.5 V~3.1 V) and long lifetime (3.4×10^{-5} s) of $SO_4^-\bullet$ [48,49]. Meanwhile, it should be noted that the activation methods of PMS make a big difference to the types of ROS, e.g., $SO_4^-\bullet$ via activation with carbon materials, $SO_4^-\bullet$ and •OH via thermal and radiation activation, $SO_4^-\bullet$ and peroxymonosulfate anion radicals ($SO_5\bullet^-$) via transition metal activation, and $\bullet O_2^-$ and $^1O_2$ via alkali activation [50]. In addition, photogenerated h^+ acts as a powerful ROS that directly oxidizes PFASs or converts H_2O/O_2 to $\bullet OH/\bullet O_2^-$, thereby generating more ROS [28]. Electrochemical processes induce the rapid generation of different ROS at the anode or facilitate electron transfer to the anode [51]. Hence, the application of light or electrical energy in AOPs has the potential to promote PFAS degradation by providing more powerful ROS or accelerating the oxidation processes. Photocatalytic or electrocatalytic AOPs are promising systems for highly effective PFAS remediation, deserving in-depth analysis and further research.

2.2. Principles of Photocatalytic AOPs for PFAS

Photocatalytic AOPs for FPAS are developed based on direct photo-degradation, achieved by breaking apart the C−F bonds using light of a specific wavelength. The direct photolysis process requires a match between the adsorption spectrum of the chemical bonds and the emission spectrum of the light, with the wavelength of the light playing a crucial role [52]. For example, PFOA has demonstrated strong UV adsorption and fast degradation at 185 nm [53,54], while light with a wavelength above 220 nm is barely absorbed by PFASs [29,55]. In photocatalytic AOPs of PFASs, the indirect photo-oxidation process is characterized by decarboxylation followed by defluorination, believed to be related to the photoinduced holes that exhibit a strong oxidizing capacity for organics. These holes work synergistically with other ROS to enhance PFAS degradation [56,57]. The system of photocatalytic AOPs consists of three components: the light, oxidant, and photocatalyst. There are two principles of PFAS degradation in photocatalytic AOPs: direct oxidation by photogenerated holes and co-oxidation with other ROS that are generated at the surface of catalysts with the assistance of the holes. The general process of PFAS degradation in photocatalytic AOPs can be described as follows: (1) Catalysts absorb light with energy (hv) equal to or greater than the band gap, which excites electrons from the valence band (VB) to the conduction band (CB), creating holes in the VB. (2) The generated electron−hole (e^-−h^+) pairs migrate to the surface of catalysts and react with the adsorbed PFAS. (3) The e^-−h^+ pairs react with precursors and generate ROS which assist in PFAS decomposition.

For example, h^+ and e^- react with H_2O and O_2, respectively, to produce •OH and $\bullet O_2^-$ (Equations (7) and (8)) [58,59].

$$h^+ + H_2O \rightarrow \bullet OH + H^+ \quad (7)$$

$$e^- + O_2 \rightarrow \bullet O_2^- \quad (8)$$

The general mechanism of photocatalytic AOPs for PFAS degradation is summarized in Figure 2, where the PFAS is represented by PFAC. Photocatalysts play a crucial role in this process, as they are responsible for generating effective ROS and binding PFAS molecules. Both of these factors determine the efficiency of degradation [46]. Therefore, the construction and structure engineering of photocatalysts have garnered significant research interest.

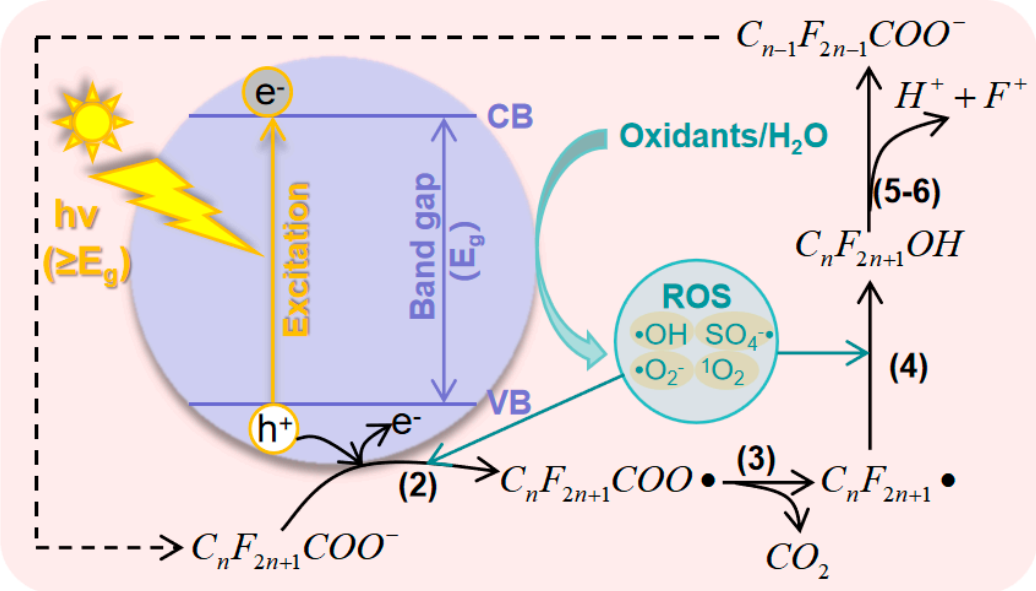

Figure 2. Mechanisms of photocatalytic AOPs for the degradation of PFASs.

2.3. Principles of Electrocatalytic AOPs for PFASs

There are two types of electrocatalytic AOPs for PFASs: direct electro-oxidation and indirect electrochemical oxidation. Direct electro-oxidation is a simple AOP that occurs on the surface of an electrode (anode) with a direct transfer of electrons. It relies on the in situ generation of ROS (e.g., •OH) or the direct transfer of electrons from the PFAS to the anode [60]. On the other hand, indirect electrochemical oxidation processes are the primary electrocatalytic AOP for organics treatment. Unlike direct electro-oxidation, electrons in this process act as mediators or assist in the generation of powerful ROS [51]. For example, the degradation of PFASs starts with the release of electrons, forming $C_nF_{2n+1}COO\bullet$ (Equation (2)); this occurs under an anode potential higher than the oxidation potential of the PFAS [61]. Additionally, electrocatalytic AOPs can produce radicals and oxidants during the electrode process. This includes •OH, which is strongly adsorbed onto the anode surface (M), as shown in Equation (9), H_2O_2 from the dimerization of •OH (Equation (10)), and ozone (O_3) from the discharge of water molecules (Equation (11)) [62]. These products are highly reactive with certain intermediate products during the decarboxylation and defluorination processes of PFASs, contributing to the efficiency of degradation.

$$M + H_2O \rightarrow M(\bullet OH) + H^+ + e^- \quad (9)$$

$$2M(\bullet OH) \rightarrow 2MO + H_2O_2 \quad (10)$$

$$3H_2O \rightarrow O_3 + 6H^+ + 6e^- \quad (11)$$

The general mechanism of electrocatalytic AOPs for PFAS degradation is illustrated in Figure 3. According to previous studies, after the formation of $C_nF_{2n+1}\bullet$ [63], there several approaches for further mineralization. Process (a) and (b) initially undergo a reaction with •OH to form $C_nF_{2n+1}OH$ (Equation (4)). In process (a), reactions from Equation (12) to Equation (13) occur [64], whereas in process (b), reactions from Equation (14) to Equation (16) take place [65,66]. Aside from •OH, other anodic ROS such as O_2 also react with $C_nF_{2n+1}\bullet$ (Equation (17)), and the oxidation product $C_nF_{2n+1}OO\bullet$ can react with other perfluoro-alkoxy radicals ($R_FCOO\bullet$) (Equation (18)). The resulting $C_nF_{2n+1}O\bullet$ then decomposes into $C_{n-1}F_{2n-1}\bullet$ for further degradation in a new cycle (Equation (19)) [63–65,67,68]. The third pathway (c) follows the reactions from Equation (17) to Equation (19).

$$C_nF_{2n+1}OH + \bullet OH \rightarrow C_nF_{2n+1}O\bullet + H_2O \quad (12)$$

$$C_nF_{2n+1}O\bullet \rightarrow C_{n-1}F_{2n-1}\bullet + CF_2O \quad (13)$$

$$C_nF_{2n+1}OH \rightarrow C_{n-1}F_{2n-1}COF + HF \quad (14)$$

$$C_{n-1}F_{2n-1}COF + \bullet OH \rightarrow C_nF_{2n}O_2H\bullet \quad (15)$$

$$C_nF_{2n}O_2H\bullet \rightarrow C_{n-1}F_{2n-1}COO\bullet + HF \quad (16)$$

$$C_nF_{2n+1}\bullet + O_2 \rightarrow C_nF_{2n+1}OO\bullet \quad (17)$$

$$C_nF_{2n+1}OO\bullet + R_FCOO\bullet \rightarrow C_nF_{2n+1}O\bullet + R_FCO\bullet + O_2 \quad (18)$$

$$C_nF_{2n+1}O\bullet \rightarrow C_{n-1}F_{2n-1}\bullet + CF_2O \quad (19)$$

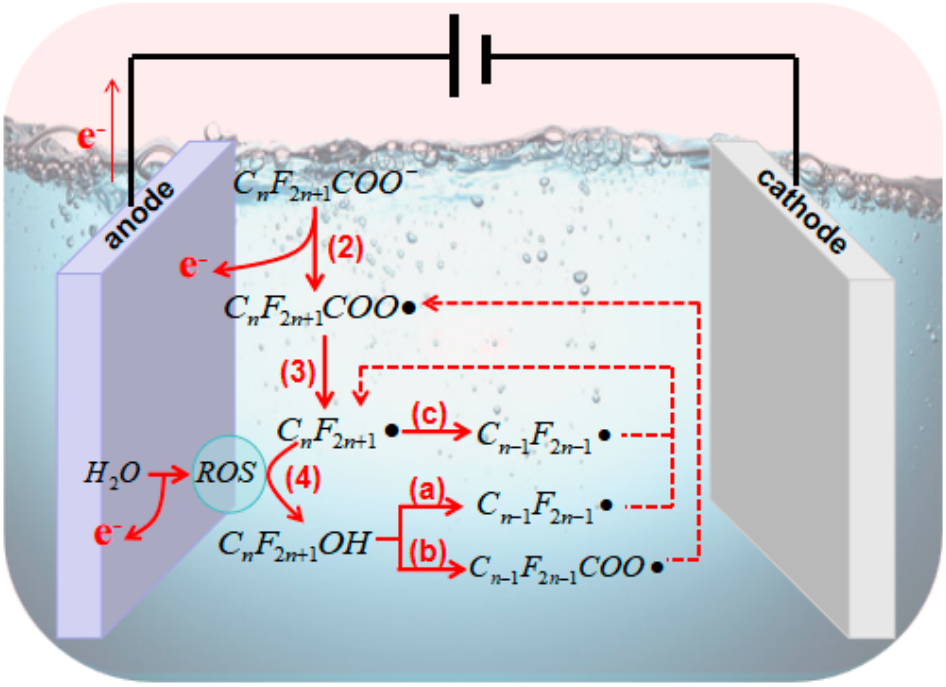

Figure 3. Mechanisms of electrocatalytic AOPs for the degradation of PFASs.

In electrocatalytic processes, oxidation primarily occurs on the anode. Therefore, the choice of anode materials (i.e., electrocatalysts) plays a crucial role in electrocatalytic AOPs for PFAS degradation. The behavior of PFAS degradation can vary depending on the type of anode material used. Anode materials are classified into two types based on the interactions

between the adsorbed •OH on the anode surface and the degradation of organics: active anodes and nonactive anodes. Active anodes, such as $Ti/SnO_2-Sb/MnO_2$ [63], have a low potential for O_2 evolution and are distinguished from non-active anodes, such as Ti/SnO_2-Sb [69], by their ability to transform M(•OH) into strong oxidants. Generally, anode materials with higher O_2-evolution potential exhibit weaker interactions between M(•OH) and their surface, but they have higher reactivity towards PFASs [51]. Therefore, the structures of anode materials are worth studying in detail to enhance the degradation of PFASs in electrocatalytic AOPs. Analyzing previous related works could contribute to further research in this area.

3. Photocatalysts in AOPs for PFAS Degradation

In photocatalytic AOPs for PFASs, catalysts play a crucial role in absorbing light energy and bandgap excitation, leading to the generation of effective ROS [46]. Based on the mechanisms of photocatalytic AOPs for PFAS degradation, strategies for constructing photocatalysts to enhance the degradation process can be summarized as follows: (1) increase the yield of ROS through element doping, introducing heterojunctions, etc. [26,70–73]; (2) increase the rate of reaction between ROS and PFASs by using composite materials and controlling their morphology [38]; and (3) expand degradation pathways by generating multiple ROS from advanced photocatalysts [74]. Currently, commonly used photocatalysts for PFAS degradation include titanium dioxide (TiO_2), indium oxide (In_2O_3), gallium oxide (Ga_2O_3), bismuth (Bi)-based materials, and their composites [27,75]. The structure engineering of these photocatalysts varies based on their intrinsic properties and elemental compositions. Therefore, the main catalysts in photocatalytic AOPs for PFAS degradation are analyzed in groups, comprising metal oxide-based materials, Bi-based materials, and other compounds and composites. Important studies on the photocatalysts used in the photocatalytic advanced oxidation of PFASs are summarized in Table 1.

3.1. Metal Oxide-Based Materials

Metal oxides, such as TiO_2, In_2O_3, and Ga_2O_3, have long been used as traditional semiconductors in the photocatalytic degradation of organics in water. These metal oxides have been extensively studied for PFAS degradation [27,46,76,77]. TiO_2-based materials, in particular, have been widely used as photocatalysts since the discovery of water splitting on a TiO_2 anode by Fujishima and Honda in 1972 [78]. Though TiO_2 has shown promise in heterogeneous photocatalysis due to its strong UV absorption, non-toxicity, and long-term photostability, it is not efficient for photocatalytic PFAS degradation. This is due to its narrow spectral range, wide bandgap (3.0 eV for the rutile phase and 3.0 eV for the anatase phase), low electron-hole separation efficiency, and poor adsorption performance. Therefore, modifications of TiO_2 are necessary to enhance its photocatalytic activity. Strategies for modification include metal/nonmetal element doping, carbon material loading, and heterostructure construction. To date, doping with Fe [79], Cu [79], Pb [24,76], Pt [80], Pd [81], Ag [82] in TiO_2 for enhanced PFAS degradation has been studied, as well as the co-doping of metals, such as Fe/Nb [70]. Metal doping involves controlling the doping amount and regulating the pH of the solution to avoid the competitive adsorption of OH^- on the catalyst surface under alkaline conditions, which may affect the PFAS treatment efficiency; see mechanism in Figure 4a. Doping non-metal elements into the crystal lattice of TiO_2 can significantly enhance its visible light activity with a reduced bandgap width by changing the positions of the CB and VB, thereby improving the degradation efficiency of PFASs in photocatalysis [83]. Carbon materials, such as carbon nanotubes [84,85], graphene-based materials [86–89], and activated carbon [90], have also been employed to enhance the photocatalytic degradation of PFASs when loaded onto modified TiO_2. These carbon materials allow for uniform dispersion of TiO_2 nanoparticles on a hydrophobic surface, leading to an increased PFAS adsorption rate and improved photocatalytic degradation with minimized risk of secondary pollution and good stability. Heterojunctions between TiO_2 and other semiconductors can enhance the electron-hole separation efficiency and

improve the photocatalytic degradation performance [26,28,71]. For instance, $Sb_2O_3-TiO_2$ heterojunctions use Sb_2O_3 nanoparticles confined within the mesoporous TiO_2 framework to adjust the band structure, increase the number of active sites for PFAS degradation, enhance UV absorption, and improve light utilization (Figure 4b) [71]. BN/TiO_2 heterojunctions facilitate charge carrier separation and enhance the degradation rate of PFOA compared to TiO_2 alone (15 times faster) [28].

In_2O_3 is a PFAS affinity material with a narrow bandgap of 2.8 eV, exceptional photocatalytic activity, and sensitivity to visible light. When compared to TiO_2, In_2O_3 has shown a remarkable 8.4-fold increase in the degradation rate coefficient of a PFAS (PFOA) under UV irradiation. These findings suggest it is a promising photocatalyst for PFAS decomposition [46]. Modifications are necessary for In_2O_3 due to its limitations, i.e., its low specific surface area and the rapid recombination of photogenerated electron-hole pairs. One effective approach is the generation of oxygen vacancies on the In_2O_3 surface, which enhances its photocatalytic performance. Additionally, nanostructures like nanospheres [42], (porous) nanosheets, and nanocubes [91,92] have been developed to provide adsorption sites for PFOA and oxygen atom binding sites in the carboxyl groups. These modifications ultimately contribute to the improved photocatalytic decomposition of PFOA. Several composite materials have been reported, such as $g\text{-}C_3N_4-In_2O_3$ [93], $CeO_2-In_2O_3$ [94], and $MnOx-In_2O_3$ [74]. Among them, the deposition of MnOx onto In_2O_3 surfaces has shown great potential; it creates abundant surface oxygen vacancies in In_2O_3, leading to the generation of active species and enhanced absorption of solar light (Figure 4c). This trend reflects the ongoing research efforts to develop photocatalytic materials for the enhanced degradation of PFASs.

Ga_2O_3 has excellent conductivity and tunable optical properties, despite its wide band-gap (4.9 eV). Studies have demonstrated its remarkable UV photocatalytic activity against PFASs, specifically in the context of PMS-assisted photocatalytic AOPs. The Ga_2O_3/PMS/UV system, with $SO_4^{-}\bullet$ and $\bullet O_2^{-}$ as key ROS, achieves 100% degradation within 60 min [38]. Current research on Ga_2O_3 focuses on structure engineering to enhance its photocatalytic activity, primarily through size and morphology control. For example, synthesizing the compound into nanoparticles, monoclinic rod-like crystals, needle-like structures, and sheet-like structures has shown promising results. Furthermore, modifications have been explored to further improve the photocatalytic activity of Ga_2O_3. One common approach is metal-doping, such as Sn-doped $\beta\text{-}Ga_2O_3$ [72] and In-doped Ga_2O_3 (Figure 4d) [95]. Metal-doping on Ga_2O_3 promotes photocatalytic degradation by enhancing absorption through the hole oxidation process. This strategy provides a new method for removing PFOA from different water sources, capitalizing on the strong bonding ability between metal-doped Ga_2O_3 and PFASs.

3.2. Bi-Based Materials

Bismuth (Bi)-based photocatalysts have emerged as one of the most promising photocatalytic materials for catalysis, primarily due to their non-toxicity, high stability, and low cost. Commonly used Bi-based compounds for PFAS photocatalytic AOPs include bismuth oxyhalides (BiOX, where X is Cl, Br, I), bismuth ferrite ($BiFeO_3$, BFO), bismuth phosphate ($BiPO_4$), and bismuth hydroxyphosphate ($Bi_3O(OH)(PO_4)_2$, BiOHP); Table 1 summarizes their photocatalytic degradation efficiency with PFASs.

BiOX is a 2D layered compound with alternating double X ion layers and Bi_2O_2 layers along the *c*-axis. An internal electric field is formed between the halide planes and Bi_2O_2 layers, promoting faster charge transfer, enhanced redox potential, and excellent photocatalytic performance for effective PFAS degradation [39]. BiOI has a narrow bandgap (E_g = 1.67~1.92 eV) and high visible light absorption, showing great potential for applications. However, the narrow bandgap leads to the easy recombination of photoinduced e^-/h+ pairs, which affects the photocatalytic activity [96]. Researchers have synthesized Br-doped BiOI ($BiOI_{0.95}Br_{0.05}$) for the photocatalytic degradation of PFOA [97]. Br doping not only increases PFOA adsorption but also expands the UV absorption range, leading to

a significant enhancement in photocatalytic activity. However, the impact of non-metals on the structural properties of the semiconductor, in terms of stability, reproducibility, loading capacity, and practical applications of BiOI, requires further investigation. BiOCl, another noteworthy semiconductor with an indirect bandgap (E_g ranging from 2.62 to 3.46 eV) possesses excellent electronic and optical properties and has become a popular photocatalytic material [98]. Researchers have successfully prepared oxygen-deficient BiOCl nanosheets employing a simple hydrolysis method [99] and a rapid microwave-assisted solvothermal method [100]. These synthesis routes enable tight carboxyl group binding at the end of PFOA through monodentate and bidentate coordination, resulting in a significant improvement in defluorination effectiveness. Notably, defluorination rates achieved through a microwave-assisted solvothermal method surpasses the conventional solvothermal method by 2.7 and 33.8 times. In addition, the incorporation of ZnAl−LDHs with BiOCl (B−BHZA) has proven to be a promising strategy, as it lowers the bandgap energy of BiOCl and introduces abundant surface defects, facilitating charge generation and separation at the heterojunction [101]. Moreover, B−BHZA extends the spectral range and enhances UV light absorption, thereby promoting the direct oxidation of PFASs by h^+ species.

BiOHP exhibits superior catalytic activity towards PFASs under UVC ultraviolet radiation compared to $BiPO_4$. This enhanced performance can be attributed to the positively charged surface of hydroxylated BiOHP, which enables the adsorption of deprotonated PFOA without relying on photocarrier reactions. However, the specific mechanism underlying this phenomenon requires further investigation [102]. It should be noted that while BiOHP effectively degrades low concentrations of PFOA in groundwater, its degradation rate is slower due to the presence of carbonate and natural organic matter [102]. To overcome this limitation, a combination of BiOHP with carbon spheres has been found to enhance its stability and catalytic performance. This synergistic effect is achieved through improved PFOA adsorption, facilitated electron transfer, and modified distribution of C−F bonds [103]. BFO is a perovskite-type mixed oxide that possesses a suitable bandgap for visible light degradation of organic pollutants. However, its photocatalytic performance is constrained, particularly for highly stable pollutants [104]. To enhance its catalytic activity, doping BFO with metals such as Pb has been investigated. The introduction of Pb provides reactive sites on the BFO surface, leading to improved performance [105]. In fact, combining Pb and reduced graphene oxide with BFO has been shown to enhance electron lifetime, facilitate reactive oxygen species generation, and promote the degradation of PFOA in water [106].

3.3. Other Compounds and Composites

In addition to metal-oxides and Bi-based materials, various photocatalysts have been employed in photocatalytic AOPs for PFAS degradation. These include metal/transition metal-based materials, metal-free materials, and modified composite materials. Qian et al. proposed a heterogeneous photocatalytic degradation mechanism for PFOA using Fe-zeolite under UVA irradiation (wavelength range: 320–420 nm) with O_2 as the terminal oxidant [107]. This Fe-zeolite catalyst, compared to homogeneous Fe^{3+}, exhibits a broader light absorption range and can oxidize Fe^{2+} to Fe^{3+} in the presence of O_2, generating reactive species that contribute to PFAS mineralization. Other photocatalysts, such as samarium doped ferrite [108] and platinum-modified indium oxide nanorods (Pt/IONRs) [109], have also demonstrated significant PFOA degradation (48.6% and 98.0%) within a short period of time (1 h) in photocatalytic AOPs. The high degradation efficiency of Pt/IONRs can be attributed to Pt loading, the rod-like structure of the catalyst, and the presence of surface oxygen vacancies, which promote light harvesting, enhance the separation efficiency of the photogenerated charge carriers, and accelerate PFOA degradation. Furthermore, a synergistic effect of metal doping and carbon material loading has been observed in Ga/TNTs@AC composites, resulting in highly enhanced PFOA degradation (Figure 4e). Carbon-based materials play a crucial role in improving photocatalytic activity by enhancing conductiv-

ity (electron transfer), as explained by Zhao et al. (Figure 4f) [110]. A few reports have investigated the use of non-metal materials for the photocatalytic degradation of PFASs. Adsorption removal methods, e.g., using magnetic mesoporous carbon nitride and powdered activated carbon, have received significant attention. Interestingly, boron nitride (BN), which is a wide bandgap semiconductor with an energy gap of 6.0 eV, has shown promising heterogeneous photocatalytic activity toward PFOA [111]. BN, subjected to ball milling, exhibits a degradation rate four times higher than that of commercial TiO_2 under UV conditions. The photodegradation of PFOA by BN follows an oxidation mechanism involving h^+, accompanied by degradation processes involving $\bullet O_2^-$ and •OH.

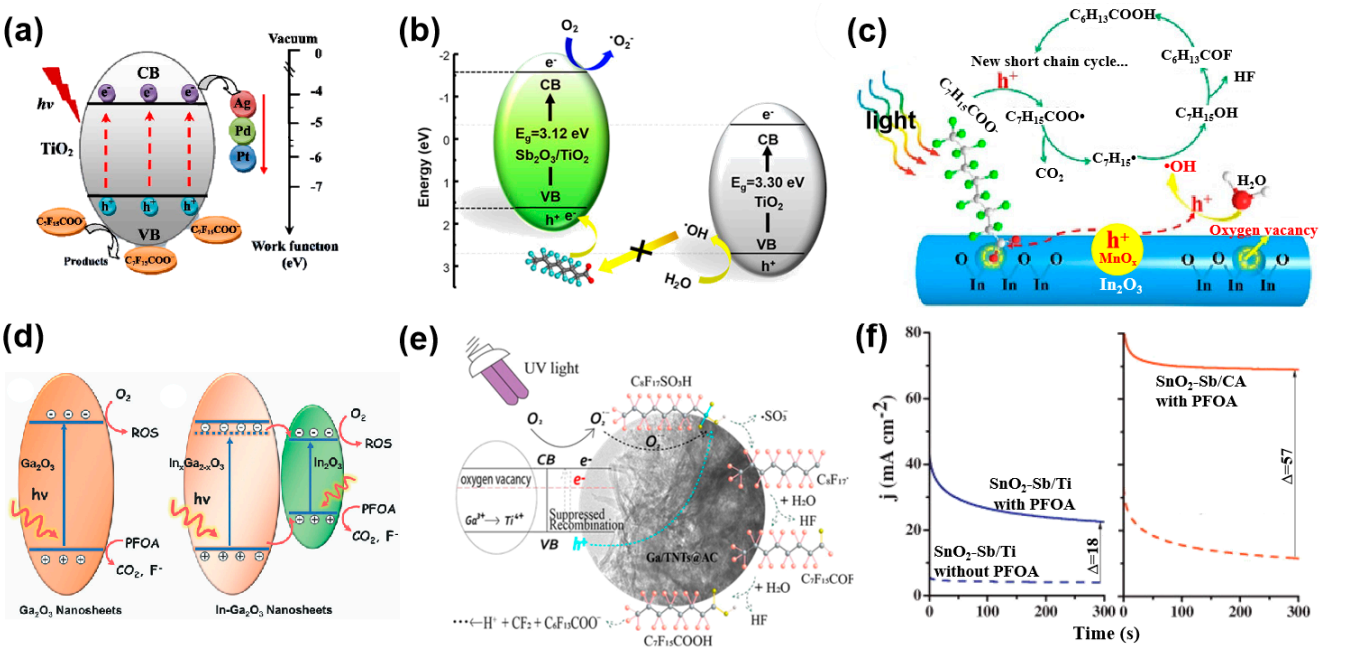

Figure 4. (**a**) The mechanism of metal-doping contributing to the photocatalytic degradation of PFOA on TiO_2 [80]. (**b**) The enhanced photocatalytic degradation of PFOA using a $Sb_2O_3-TiO_2$ heterojunction [71]. (**c**) MnO_x modification enhances the photocatalytic degradation of PFOA on In_2O_3 by introducing oxygen vacancies and generating more ROS [74]. (**d**) The band structures and photodegradation mechanism of PFOA on Ga_2O_3, with and without In-doping [95]. (**e**) The composite material Ga/TNTs@AC exhibits enhanced photodegradation of PFOSs through a synergistic effect of metal-doping and carbon material-loading [112]. (**f**) The enhanced photocatalytic degradation of PFOA has been achieved by loading a catalyst onto carbon aerogel (CA) over Ti [110].

To conclude, various strategies in material construction and structure engineering have been developed to enhance the photodegradation of PFASs. These strategies aim to increase the adsorption of PFAS molecules onto catalysts or promote the generation of ROS. These approaches include:

(1) The construction of defect sites through the introduction of oxygen vacancies and element doping. Defect sites serve as active sites for adsorption and catalytic reactions. Additionally, they broaden the light absorption range and enhance the light absorption capability by modifying the electronic and band structure.

(2) The construction of heterojunctions by synthesizing composite materials. This involves combining two or more semiconductors with suitable band structures. The overlapping or coupling of these semiconductors enables the migration and separation of photo-generated charge carriers, effectively suppressing the recombination of electrons and holes. This leads to an enhanced photocatalytic efficiency.

(3) The deposition of photocatalysts onto carbon material. The use of carbon nanomaterials, which possess a larger surface area and a porous structure, provides more active adsorption sites and improves catalyst stability. Furthermore, carbon materials

facilitate interface charge transfer, prolong the lifetime of photo-generated charged carriers, and enhance visible light absorption by adjusting the band gap and acting as sensitizers.

(4) The modulation of the crystal plane structure and electronic structure through the adjustment of the catalyst preparation methods. Exposing crystal planes with high surface energy and reactivity facilitates the separation of photo-generated electrons and holes, thus enhancing the photocatalytic activity of the catalysts.

Table 1. Summary of photocatalysts in photocatalytic AOPs for PFAS degradation.

	Photocatalysts	Target PFAS	$[PFAS]_0$	Experimental Conditions [Catalyst], Light Wavelength/Strength, pH	Removal Efficiency	Structural Engineering	Ref.
Metal oxide-based materials	TiO_2	PFOA	59 mg·L^{-1}	0.25 g·L^{-1}, 400~770 nm/300 W, pH = 3 TiO_2/UV/PMS system, ([PMS] = 0.75 g·L^{-1})	100% (8 h)	none	[75]
	TiO_2 nanotubes	PFOA	50 mg·L^{-1}	0.125 g·L^{-1}, 254 nm/400 W, pH = 4	85% (24 h)	morphology control	[113]
	Pb−TiO_2	PFOA	50 mg·L^{-1}	0.5 g·L^{-1}, 254 nm/400 W, pH = 5	50% (1.3 h)	metal-doping	[76]
	Pt−TiO_2	PFOA	60 mg·L^{-1}	0.5 g·L^{-1}, 365 nm/125 W, pH = 3	100% (7 h)	metal-doping	[80]
	Cu−TiO_2	PFOA	50 mg·L^{-1}	0.5 g·L^{-1}, 254 nm/100 W, pH = 5	91% (12 h)	metal-doping	[79]
	Sb_2O_3/TiO_2	PFOA	10 mg·L^{-1}	2.5 g·L^{-1}, 200~280 nm/4 W, pH = 4.4	81.7% (2 h)	heterojunction	[71]
	BN/TiO_2	PFOA	100 μM	0.5 g·L^{-1}, 254 nm/4 W, pH = 3.2	97.6% (4 h)	heterojunction	[28]
	PLA−3DP TiO_2	11PFASs	ng·L^{-1}~mg·L^{-1}	N/A, 280~400 nm/1.0 mW, pH = 7.1 ± 1	80% (24 h)	morphology control	[25]
	TiO_2−MWCNTs	PFOA	30 mg·L^{-1}	1.6 g·L^{-1}, 365 nm/300 W, pH = 3	94% (8 h)	carbon material loading	[84]
	MWCNTs/C−TiO_2	PFOA	2 mg·L^{-1}	1.0 g·L^{-1}, 420 nm/300 W, pH = 4.65	90% (3.5 h)	morphology control	[85]
	rGO/TiO_2	PFOA	100 mg·L^{-1}	1.0 g·L^{-1}, 200~600 nm/150 W, pH = 7	93 ± 7% (12 h)	morphology control	[89]
	Ti_3C_2/TiO_2	PFOA	20 μM	0.2 g·L^{-1}, 254 nm/4.5 W, pH = 3	>99.9% (16 h)	heterojunction	[114]
	In_2O_3	PFOA	100 μM	0.5 g·L^{-1}, 254 nm, pH = 4.2	80% (4 h)	none	[46]
	g-C_3N_4/In_2O_3	PFOA	200 mg·L^{-1}	0.4 g·L^{-1}, 254 nm/500 W, pH = N/A	91% (1 h)	carbon material loading	[93]
	In_2O_3−GRs	PFOA	30 mg·L^{-1}	0.4 g·L^{-1}, 254 nm/15 W, pH = N/A	100% (3 h)	carbon material loading	[115]
	CeO_2/In_2O_3	PFOA	100 mg·L^{-1}	0.4 g·L^{-1}, 254nm/500 W, pH = 2.84	100% (1 h)	heterojunction	[94]
	$MnO_x-In_2O_3$	PFOA	50 mg·L^{-1}	0.5 g·L^{-1}, visual light/500 W, pH = 3.8	99.8% (3 h)	heterojunction	[74]
	β-Ga_2O_3	PFOA	10 mg·L^{-1}	0.5 g·L^{-1}, 254 nm/50 W, pH = 7	98.8% (1.5 h)	none	[77]
	In−Ga_2O_3	PFOA	20 mg·L^{-1}	0.5 g·L^{-1}, 320 nm/200 W, pH = 7	100% (1 h)	metal-doping	[95]
	ZnO	PFOA	10 mg·L^{-1}	0.2 g·L^{-1}, 254 nm/28 W, pH = 4.5 ZnO/UV/O_3 system	70.5% (4 h)	none	[116]
	ZnO−rGO	PFOA	10 mg·L^{-1}	0.2 g·L^{-1}, 254 nm, pH = N/A O_3/UV/ZnO−rGO/$S_2O_8^{2-}$ system	99.2% (4 h)	carbon material loading	[117]
Bi-based materials	BiOX/TiO_2	PFOA	10 mg·L^{-1}	0.2 g·L^{-1}, 254 nm/30 W, pH = 7	100% (8 h)	carbon material loading	[26]
	BiOCl nanosheets	PFOA	0.02 mM	0.5 g·L^{-1}, 254 nm/10 W, pH = 4.8	59.3% (24 h)	morphology control	[99]
	$BiOI_{0.95}Br_{0.05}$	PFOA	20 mg·L^{-1}	0.4 g·L^{-1}, 254 nm/300 W, pH = 7	96% (2 h)	crystal facet control	[97]
	BiOI/Bi_5O_7I	PFOA	15 mg·L^{-1}	0.5 g·L^{-1}, 400~760 nm/800 W, pH = 3.0	80% (6 h)	heterojunction	[73]
	BiOCl/$BiPO_4$	PFOA	20 mg·L^{-1}	0.5 g·L^{-1}, 254 nm/2 W, pH = 7	100% (45 h)	heterojunction	[118]
	BiOHP	PFOA	0.5 mg·L^{-1}	1.8 g·L^{-1}, 254 nm/18 W, pH = 4.0	70%(20 min)	morphology control	[102]
	BiOHP/CS	PFOA	0.2 mg·L^{-1}	1.0 g·L^{-1}, 254 nm/18 W, pH = 7.0	>90% (1 h)	carbon material loading	[103]
Other composites	Fe−BEA35	PFOA	48 μM	1 g·L^{-1}, 365 nm/4 W, 254 nm/4 W, pH = 3	>99% (24 h)	metal-doping + morphology control	[107]
	Pt/IONRs	PFOA	200 mg·L^{-1}	0.4 g·L^{-1}, 254 nm/500 W, pH = 1.85	98% (1 h)	metal-doping + morphology control	[119]
	Fe/TNTs@AC	PFOA	0.1 mg·L^{-1}	1.0 g·L^{-1}, 254 nm/21 W, pH = 3.0	90% (4 h)	metal-doping + carbon material loading	[90]
	Ga/TNTs@AC	PFOS	100 μg·L^{-1}	1 g·L^{-1}, nm/200 W, pH = 7.0 ± 0.1	75% (4 h)	metal-doping + carbon material loading	[112]
	Zn−AlLDHs −BiOCl	PFOA	0.5 mg·L^{-1}	0.5 g·L^{-1}, <350 nm/50 W, pH = 2.0	90% (6 h)	metal-doping + morphology control	[101]
	Pb−$BiFeO_3$ /rGO	PFOA	50 mg·L^{-1}	0.1·L^{-1}, 254 nm/5 W, pH = 2.0	69.6% (8 h)	metal-doping + carbon material loading	[106]

4. Electrocatalysts in AOPs for PFAS Degradation

Electrocatalysts assume the role of electrode materials in electrocatalytic AOPs, where electrochemical oxidations for PFAS degradation occur on their surface. The key factors determining the efficiency of anodic oxidation in electrocatalytic AOPs include the production of ROS, the rate of mass transfer from the bulk solution to the electrode surface, the availability of active sites on the electrode surface for degradation reactions of PFASs and their transformations, as well as the stability and current transfer efficiency of the anode materials [22,120–122]. Based on these factors, the electrocatalytic performance of anode materials can be improved by increasing the number of active sites, enhancing the electron transfer rate, accelerating mass transfer, and employing strategies such as introducing defects, elemental doping, surface modifications, designing the microstructure of the electrode, and exposing preferred crystal facets [71,123,124]. Currently, a wide variety of photocatalysts are used for PFAS degradation, with commonly employed anode materials including boron-doped diamond (BDD), tin oxide (SnO_2), lead oxide (PbO_2), and others [63,66,125]. To clarify the strategies used in constructing materials for different groups of electrocatalysts, a classified analysis of recently studied electrocatalytic materials for PFAS degradation on the anode is provided, specifically focusing on BBD-based electrodes, metal oxide-based materials, and other hybrids materials. Important research on catalysts for the electrocatalytic degradation of PFASs is summarized in Table 2.

4.1. BDD-Based Materials

Boron-doped diamond (BDD) is a one of the most frequently used anode materials in the electrocatalytic degradation of PFASs, owing to its wide operational potential window, excellent chemical stability, and high oxidation potential (2.7 V vs. SHE) [65,126,127]. The BDD electrode plays a crucial role in the direct electrochemical oxidation of PFASs at low current densities, rather than relying on the •OH oxidation process at high current densities [11,128]. BDD films have been proven to be effective anodic electrocatalysts for PFOS degradation [127], with electron transfer from PFOS to the anode resulting in the formation of final products such as SO_4^{2-}, F^-, CO_2 and a small amount of trifluoroacetic acid. However, the widespread application of BDD as an anode material in electrocatalytic AOPs for PFASs is limited due to its high cost and a lack of suitable electrode substrates for BDD. Metals and nonmetals like Ta, Nb, W, and Si have been investigated as BDD substrates, and Si/BDD has been found to be a cost-effective option for PFOS degradation (>90%) [123,129]. Moreover, B/N co-doped diamond (BND) has been developed as an anode for sulfate-activated electrocatalytic AOPs for PFASs [120]. B/N co-doping enhances ROS generation by increasing the number of active sites, thereby promoting the electrochemical activation of the sulfate solution and PFAS degradation, as depicted in Figure 5a. However, the electrocatalytic activity of BDD is hindered by the occurrence of fluorination on the surface through the binding of fluoride ions in the solution; to date, only a handful of reports have addressed this issue [126,130]. Therefore, further research should be conducted on the surface engineering of BDD to reduce F^- adsorption on the anode surface and thereby enhance its efficiency in electrocatalytic PFAS degradation.

4.2. Metal Oxide-Based Materials

The utilization of metal oxides as electrode materials has revealed the drawbacks associated with metal electrodes, such as lower oxygen evolution overpotential and susceptibility to oxidation. Additionally, it has made it possible to overcome the limitations of BDD electrodes, including low conductivity and low efficiency in terms of utilizing •OH radicals [131]. Currently, metal oxides commonly used as electrode materials include SnO_2, PbO_2, TiO_2, MnO_2, and others. Among these, SnO_2 and PbO_2 demonstrate outstanding electrocatalytic oxidation performance, with a higher overpotential of O_2 evolution, making them suitable for the degradation of organics.

SnO_2, a semiconductor with a bandgap of 3.5eV, faces challenges in its direct use as an electrode material due to its high resistance. However, its conductivity can be im-

proved through doping [22,122,132], particularly with antimony (Sb) [63,125]. In addition, SnO_2-Sb electrodes exhibit a high oxygen evolution potential, which contributes to their extensive application in PFAS degradation [63,65,110]. By doping Ti/SnO_2-Sb with multiple metals, a PFOA removal rate of 93.3% can be achieved [63,65]. It is important to note that the presence of SO_4^{2-} in the solution can cover the active sites on the electrode. This reduces the production of •OH radicals, subsequently decreasing the PFOA removal rate [110]. Moreover, F-doped SnO_2 electrodes (Ti/SnO_2-F) demonstrate a higher oxygen evolution potential and better catalytic activity than Ti/SnO_2-Sb electrodes. This can be attributed to the smooth surface of F-doped SnO_2 electrodes, which minimizes electrolyte infiltration and ensures electrode stability [122]. Furthermore, a Ti/SnO_2-Bi electrode achieved a 99% PFOA removal rate within 2 h [65]. However, the high anode potential (3.37 V) led to the primary degradation mechanism being the direct oxidation of PFOA on the anode through decarboxylation, resulting in inferior performance for PFOS degradation. Apart from Ti, carbon-based materials hold promise as substrates for metal oxide-based electrocatalysts. For example, carbon aerogel (CA)$/SnO_2-Sb$ electrodes exhibit a significantly improved degradation rate for PFOA, i.e., 3.5 times higher than for Ti/SnO_2-Sb electrodes [110].

PbO_2 anodes offer several advantages for efficient PFAS degradation, such as low processing costs, simple preparation, high conductivity, and a high oxygen evolution potential [133,134]. However, the issue of PbO_2 detachment in Ti/PbO_2 electrodes hampers their stability. To address this, $Ti/SnO_2-Sb/PbO_2$, and TiO_2-Nanotubes (NTs)$/Ag_2O/PbO_2$ electrodes have been developed, effectively enhancing the stability and electrochemical degradation capability with the assistance of an interlayer [124,135,136]. A study was conducted [137], highlighting the contribution of interlayer metal/metal oxide anodes to the efficiency of PFOS degradation (Figure 5b). However, PbO_2 electrodes are susceptible to Pb^{2+} leaching [133,134]; this can be mitigated through doping with elements to reduce the grain size, increase the electroactive surface area, improve the oxygen evolution potential, and enhance electron migration ability. Doping with cerium (Ce), ytterbium (Yb), and zirconium (Zr) has resulted in removal rates of over 88% for PFOA [67,68,138]. A $Ti/SnO_2-Sb/PbO_2-Ce$ electrode exhibited removal rates of over 92% for PFDA and PFNA. It is worth noting that the electrochemical degradation rate of PFASs on Ti/SnO_2-based electrodes is influenced by the chain length, emphasizing the need to tailor the catalyst according to the PFAS chain structure [63,67,139]. Carbon-based materials also contribute to electrocatalytic PFAS degradation as substrates for PbO_2. For instance, a 3D graphene (3DG)-PbO_2 anode obtained through electro-deposition exhibited a degradation rate constant for PFOS that was 2.33 times higher than that of PbO_2 anodes [140]. This can be attributed to the porous nanostructures, resulting in a larger specific surface area and multiple electronic transfer channels (Figure 5c) in the anode. Similarly, doping tetrafluoroethylene (PTFE) into PbO_2 enhances the mass transfer and •OH generation capacity. $PTFE-PbO_2$ provides more active sites and a faster electron transfer rate, contributing to outstanding degradation efficiency [22].

Other metal oxide-based electrocatalysts, such as Ti_4O_7, have recently been studied as promising electrocatalysts. The use of a porous Magnéli phase Ti_4O_7 membrane as an anode has been shown to improve the electro-degradation efficiency for PFOS [141]. This improvement can be attributed to the increased electroactive surface area and enhanced interphase mass transfer facilitated by the Ti_4O_7 reactive electrochemical membrane (REM). In addition, doping Ti_4O_7 with metal ions (e.g., Ce^{3+}) and metals (e.g., amorphous Pd) has proven to be effective in enhancing the electrocatalytic degradation. Ce^{3+} ions promote ROS generation and electron transfer (Figure 5d) [121], while the high oxidation state and electron-deficient 5d orbitals of amorphous Pd clusters facilitate the efficient extraction of electrons from PFOA [142]. The abundant Pd−O species on the surface serve as channels for the transfer of electrons from PFOA to the electrode, thereby enhancing the anodic oxidation capability. Furthermore, Wang et al. developed Ti^{3+}/TiO_2-nanotube arrays (NTA) with both metal ion doping and a 3D structure construction. This approach achieved

enhanced electron and mass transfer, resulting in efficient electrocatalytic degradation for PFOA (Figure 5e) [21].

4.3. Other Compounds and Composites

Composites and hybrids used as anode materials for the electrocatalytic degradation of PFASs can take various forms, employing different mechanisms to improve electrocatalysis performance. However, most of the composites or hybrids used as electrocatalysts are either BDD-based or metal oxide-based materials, as discussed above. Furthermore, there are only a few studies available on this topic, leaving ample room for further research [19,20,143]. In terms of electrode materials, one scarcely investigated type which has demonstrated high reactivity and chemical robustness is the multifunctional single-atom catalyst (SAC). SACs show promise in electrocatalytic PFAS degradation [144]. In a recent study, a Co-based SAC ($Co-CN_2$) immobilized with Fe_2O_3 was reported as a highly efficient electrocatalyst for PFOA degradation. This was attributed to the construction of catalytic Fenton reactions with locally generated H_2O_2 (Figure 5f) [20]. In addition to anode materials, research on cathodes for enhanced electrocatalytic AOPs in PFAS degradation has also been conducted. These studies rely on the synergistic effect of cathodic electro-AOPs (Fenton) and anodic oxidation. For example, an Fe–Mn-based catalyst was developed by doping it into CA [143]. In this case, Fe and Mn were used as Fenton catalysts, providing better distribution of active sites for enhanced •OH generation. As a result, a 97% removal rate of PFOA was achieved with 4 h of electrocatalysis.

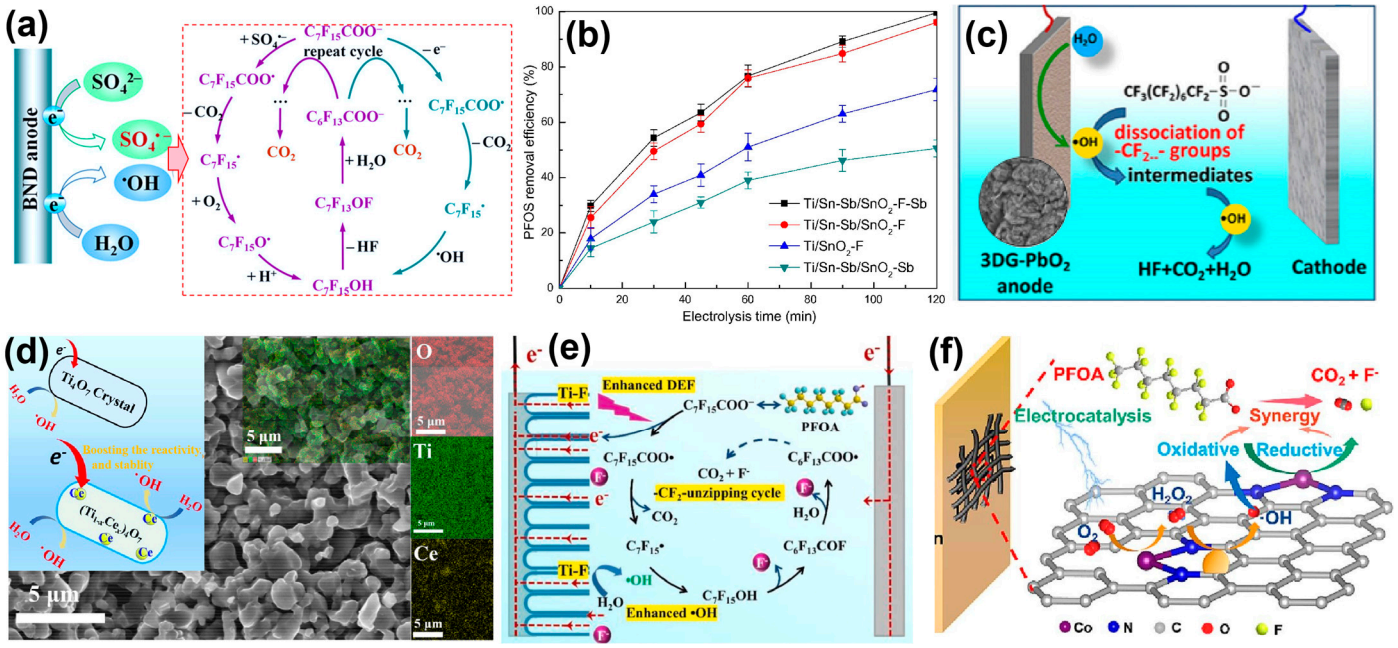

Figure 5. (**a**) The use of element (B/N)-doped diamond (BND) as an anode promotes PFOS electrodegradation by generating ROS [120]. (**b**) The Sn−Sb interlayer and F doping contribute to the degradation of PFOS on a Ti/SnO_2 anode [137]. (**c**) The 3DG-PbO_2 composite anode effectively degrades PFOSs due to its strong ROS generation capacity, abundant active sites, and small charge-transfer resistance [140]. (**d**) Ce^{3+} doping enhances the electrocatalytic degradation of PFOS on a Ti_4O_7 anode by increasing ROS generation and electron transfer [121]. (**e**) Enhanced electron and mass transfer on a Ti^{3+}/TiO_2-NTA anode for PFOA mineralization is achieved through metal-doping and a 3D nanotube structure [21]. (**f**) The nearly complete mineralization of PFOA on $Co-CN_2-Fe_2O_3$ composites is attributed to the synergistic effect of single-atom catalysis on $Co-CN_2$ and Fenton catalysis on Fe_2O_3 [20].

Based on a comprehensive analysis of key factors in the electrocatalytic oxidation of organics, including the generation of ROS, mass/charge transfer efficiency, and electrode

stability, the structural engineering of electrocatalysts for effective PFAS degradation can be summarized as follows:

(1) Enhancing the yield of ROS on the electrode by doping a specific functional substance onto the surface. Doping helps optimize the crystalline phase of the catalytic electrodes, promoting a more compact arrangement of particles and effectively enhancing the electrode's ability to generate physically adsorbed ROS species.

(2) Improving the surface mass transfer efficiency of the electrode through metal loading and the implementation of three-dimensional nanostructures. Metal-doping is an important strategy for reducing and improving electron transfer. Constructing 3D nanostructures on the electrode surface increases the specific surface area and active sites, thereby enhancing the migration of PFASs toward the electrode and improving their adsorption efficiency.

(3) Enhancing the stability of the electrode by introducing functional intermediate layers. Incorporating the intermediate layer strengthens the interaction between the active layer and the substrate, preventing the detachment of the active layer, improving electrode stability, and extending the electrode's lifespan.

Table 2. Summary of electrocatalysts in electrocatalytic AOPs for PFAS degradation.

	Electrocatalysts	Target PFAS	$[PFAS]_0$ (Electrolyte Solution)	Experimental Conditions Surface Area (S), Interelectrode Gap (L), Electric Current Density (J)	Removal Efficiency	Structural Engineering	Ref.
BDD-based materials	BDD	PFOS	0.4 mM (10 mM $NaClO_4$)	S = 25 cm^2, L = 2 mm, J = 20 $mA{\cdot}cm^{-2}$, T = 22 °C, pH = 4	50% (5.3 min)	none	[127]
	BDD (high boron)	PFOA +PFOS	0.1 mg L^{-1} (100 mM PBS)	S = 10.5 cm^2, L = 2.5 cm, J = 75 $mA{\cdot}cm^{-2}$, T = 20~25 °C, pH = 7.8	80%PFOA, 78%PFOS	doping (B)	[11]
	BND	PFOA	50 mg L^{-1} (0.05 M Na_2SO_4)	S = 10.5 cm^2, L = 2.5 cm, J = 4 $mA{\cdot}cm^{-2}$, pH = 4.8	77.4% (3 h)	doping (N)	[120]
	Si/BDD	PFOA	0.2 mg L^{-1} (0.4 g L^{-1} Na_2SO_4)	S = 81 cm^2, L = 1 cm, J = 25 $mA{\cdot}cm^{-2}$, pH = 11	>90% (1 h)	metal-doping	[129]
	Ti/BDD	PFCAs	0.25 mM (10 mM $NaClO_4$)	S = 25 cm^2, L = 1.5 cm, J = 10 $mA{\cdot}cm^{-2}$, pH = 3	>95% (3 h)	metal-doping	[66]
Metal-oxide based materials	Ti^{3+}/TiO_2−NTA	PFOA	50 mg L^{-1} (20 mM Na_2SO_4)	S = 25 cm^2, L = 1 cm, J = 2 $mA{\cdot}cm^{-2}$, pH = 3~11	98.1% (1.5 h)	doping + morphology control	[21]
	Ti/SnO_2−Sb	PFOA	100 mg L^{-1} (10 mM $NaClO_4$)	L = 1 cm, J = 10 $mA{\cdot}cm^{-2}$, T = 25 °C, pH = 5	90.3% (1.5 h)	co-doping	[63]
	Ti/SnO_2−Sb/PbO_2				91.1% (1.5 h)	metal-doping +intercalation	
	Ti/SnO_2−Sb/MnO_2				31.7% (1.5 h)	metal-doping +intercalation	
	Ti/SnO_2−Sb/Bi_2O_3	PFOS	20 mg L^{-1} (1.4 g L^{-1} $NaClO_4$)	S = 17.64 cm^2, J = 6.8 $mA{\cdot}cm^{-2}$, T = 32 °C, pH = 6.94	23.8% (3.5 h)	metal-doping +intercalation	[145]
	Ti/SnO_2−F	PFOA	100 mg L^{-1} (10 mM $NaClO_4$)	S = 25 mm^2, L = 1 cm, J = 100 $mA{\cdot}cm^{-2}$, T = 25 °C, pH = 7	96.5% (0.5 h)	co-doping	[122]
	SnO_2−Sb/CA	PFOA	100 mg L^{-1} (0.1 M Na_2SO_4)	S = 5 cm^2, L = 1 cm, J = 20 $mA{\cdot}cm^{-2}$, T = 20 °C, pH = 7	91% (5 h)	metal-doping +carbon material loading	[110]
	Ti/SnO_2−Sb−Bi	PFOA	50 mg L^{-1} (1.4 g L^{-1} $NaClO_4$)	S = 11.33 cm^2, L = 10 mm, J = 22 $mA{\cdot}cm^{-2}$, pH = 4.71	>99% (2 h)	co-doping	[65]
	Ti/Sn−Sb/SnO_2−F −Sb	PFOA	100 mg L^{-1} (10 mM $NaClO_4$)	S = 25 mm^2, L = 1 mm, J = 20 $mA{\cdot}cm^{-2}$, T = 25 ± 3 °C, pH = 2	99% (2 h)	co-doing +intercalation	[137]
	3DG−PbO_2	PFOS	50 mg mL^{-1} (0.05 M Na_2SO_4)	J = 30 $mA{\cdot}cm^{-2}$, T = 30 °C, pH = 7	96.17% (2 h)	carbon material loading	[140]
	Ceramic/PbO_2 −PTFE	PFOA	20 mg mL^{-1} (15 mM Na_2SO_4)	S = 20.6 cm^2, L = 2 cm, J = 15 $mA{\cdot}cm^{-2}$, T = 25 °C, pH = 7	98.9% (5 h)	doping + loading	[22]
	Ti/TiO_2NTs /Ag_2O/PbO_2	PFOS	0.0929 mM (1.4 g L^{-1} Na_2SO_4)	S = 12 cm^2, L = 10 mm, J = 30 $mA{\cdot}cm^{-2}$, T = 30 ± 2 °C	74.87% (1.5 h)	metal-doping +morphology control	[146]

Table 2. *Cont.*

	Electrocatalysts	Target PFAS	$[PFAS]_0$ (Electrolyte Solution)	Experimental Conditions Surface Area (S), Interelectrode Gap (L), Electric Current Density (J)	Removal Efficiency	Structural Engineering	Ref.
Metal-oxide based materials	Magnéli phase Ti_nO_{2n-1}	PFOS	2.0 μM (100 mM Na_2SO_4)	S = 4 cm^2, L = 10 cm, J = 10 mA·cm^{-2}, T = 25 ± 1 °C, pH = 6	98.30 ± 0.51% (2 h)	morphology control	[141]
	Porous Ti_4O_7	PFOA PFOS	0.5 mM PFOA, 0.1 mM PFOS (0.25 M Na_2SO_4)	S = 1 cm^2, L = 1.5 cm, J = 10 mA·cm^{-2}, T = 25 ± 1 °C,	99.9% PFOA 9.1% PFOS (3 h)	morphology control	[147]
	Ti_4O_7 REM	PFOA +PFOS	10 μM (100 mM K_2HPO_4)	S = 0.5 cm^2, anode potential = 3.6 V/SHE, pH = 7	>99.9%	morphology control	[148]
	Ce-doped Ti_4O_7: $(Ti_{1-x}Ce_x)_4O_7$	PFOS	20 nM (10 mM Na_2SO_4)	S = 9 cm^2, L = 5 mm, J = 20 mA·cm^{-2}, pH = 7	>83.3% (2 h)	metal-doping	[121]
	Pd/Ti_4O_7	PFOA	0.12 mM (50 mM Na_2SO_4)	S = 25 cm^2, V = 30 mL, J = 10 mA·cm^{-2}, T = 25 ± 1 °C, pH = 7.2	>90% (1 h)	metal-doping	[142]
	Mixed metal oxide (MMO)	PFOA +PFOS	5 mg L^{-1} (500 mg/L Na_2SO_4)	S = 100 cm^2, L = 16 mm, J = 10 mA·cm^{-2}, pH = 7.4	>90% (8 h)	morphology control	[149]
	$LaNi_xY_{1-x}O_3$ (Y = Fe/Cu/Co/Sr)	PFOA	0.25 mM (0.05 M Na_2SO_4)	L = 3 cm, J = 20 mA·cm^{-2}, pH = 5, 1.0 mM $FeSO_4$	90% (Y = Sr, 2.5 h)	crystal facet control	[150]
Other composites	Mxene-based membrane	PFBA +PFOA	1 μg/L (0.1 M Na_2SO_4)	S = 12.56 cm^2, L = 10 mm, J = 10 mA·cm^{-2}, pH = 7.00 ± 0.10	>99% (3 h)	morphology control	[19]
	$Co-CN_2-Fe_2O_3$	PFOA	1.9 mg L^{-1} (0.05 M Na_2SO_4)	S = 0.2475 cm^2, J = 2.2 mA·cm^{-2}, T = 25 °C, pH = 2	70% (30 min)	metal-doping +morphology control	[20]
	Fe−Mn/CA	PFOA	50 mg mL^{-1} (50 mM Na_2SO_4)	S = 7.0 cm^2, L = 2 cm, J = 2.85 mA·cm^{-2}, T = 25 °C, pH = 3	97% (4 h)	co-doping +morphology control	[143]

5. Conclusions and Perspectives

This review presents the latest research on photo/electro-catalytic advanced oxidation processes for the degradation of PFASs. It extensively analyzes the mechanisms and pathways of photocatalytic and electrocatalytic degradation of PFASs. Based on this, the current research status of photocatalysts and electrocatalysts was systematically reviewed. Material modification methods for enhancing PFAS degradation in photocatalytic and electrocatalytic AOPs are summarized as follows:

(1) For catalysts in the photocatalytic oxidation of PFAS systems, current research primarily focuses on improving catalyst activity by addressing the rapid recombination of photogenerated $e^- - h^+$. Methods include introducing surface defects or oxygen vacancies, metal-doping, heterojunction construction, and crystal facet regulation [21,26,28,39,71,74,96,101]. Furthermore, material composites and morphology regulation have been utilized to enhance reaction probabilities between PFASs and active groups, effectively enhancing the efficiency of PFAS degradation [25,28,40,104].

(2) For catalysts in the electrocatalytic oxidation of PFAS systems, current research mainly focuses on increasing the yield of active groups through various methods [21,85,94]. Additionally, enhancing the efficiency of electron transfer and mass transfer processes is achieved through metal loading and constructing nano 3D structures [43,85,124,140]. The stability of electrodes is also improved through the construction of intermediate layers [63,145].

The challenges and prospects regarding the current state of development for these methods can be summarized as follows:

(1) Regarding catalysts: Research on photocatalytic materials aims to develop novel catalysts through the combination of various modification strategies. The goal is to enhance catalyst adsorption efficiency, increase the concentration of active components on the material surface, and improve light utilization, thereby promoting the efficient transfer and separation of photogenerated charges on the photocatalytic material surface [28,35,71,90]. Research on electrocatalytic materials mainly focuses

on developing efficient, inexpensive, and highly stable anode materials to enhance the surface activity sites of electrodes, thereby effectively enhancing PFAS degradation.

(2) Beyond catalysts: In-depth study of other factors in advanced oxidation processes aims to enhance degradation efficiency of PFAS through system optimization. This includes adjusting the solution chemistry [75], adopting various strategies for synergistic catalytic oxidation [83], and conducting research on photo/electrocatalytic treatment technology to improve the utilization of catalyst materials and reduce treatment costs [30].

(3) Current research on photo/electrocatalytic oxidation for PFAS degradation is predominantly based on ideal reaction systems. However, it is necessary to consider the actual wastewater environment, including pH, natural organic matters, coexisting ions, and the competition adsorption of degradation intermediates on the catalyst surface. Research on the competitive reactions of PFASs and coexisting substances with effective ROS should be conducted to promote the practical application of photo/electrocatalytic degradation of PFASs [59,151,152].

Author Contributions: Conceptualization, X.C. and M.M.; resources, T.Y., X.Y., writing–original draft preparation, X.C., T.Y.; writing–review and editing, M.M., X.Y. and S.D.; supervision, X.C. and M.M.; funding acquisition, X.C. All authors have read and agreed to the published version of the manuscript.

Funding: This work was funded by National Natural Science Foundation of China (No. 22306096), Natural Science Foundation of the Higher Education Institutions of Jiangsu Province (No. 22KJB610003) and the China Postdoctoral Science Foundation (No. 2023M731592).

Data Availability Statement: Data sharing is not applicable to this article. No new data were created or analyzed in this study.

Conflicts of Interest: The authors declare no competing financial interest.

References

1. Sadia, M.; Nollen, I.; Helmus, R.; ter Laak, T.L.; Béen, F.; Praetorius, A.; van Wezel, A.P. Occurrence, Fate, and Related Health Risks of PFAS in Raw and Produced Drinking Water. *Environ. Sci. Technol.* **2023**, *57*, 3062–3074. [CrossRef] [PubMed]
2. Dong, C.; Huang, F.; Deng, H.; Schaffrath, C.; Spencer, J.B.; O'Hagan, D.; Naismith, J.H. Crystal structure and mechanism of a bacterial fluorinating enzyme. *Nature* **2004**, *427*, 561–565. [CrossRef] [PubMed]
3. United States Environmental Protection Agency. Interim Updated PFOA and PFOS Health Advisories. 2022. Available online: https://www.epa.gov/sdwa/drinking-water-health-advisories-pfoa-and-pfos (accessed on 15 June 2022).
4. Eurofins. PFAS in the Revised Drinking Water Directive (DWD). Available online: https://www.eurofins.se/tjaenster/miljoe-och-vatten/nyheter-miljo/pfas-in-the-revised-drinking-water-directive-dwd/ (accessed on 26 May 2023).
5. Gagliano, E.; Sgroi, M.; Falciglia, P.P.; Vagliasindi, F.G.A.; Roccaro, P. Removal of poly- and perfluoroalkyl substances (PFAS) from water by adsorption: Role of PFAS chain length, effect of organic matter and challenges in adsorbent regeneration. *Water Res.* **2020**, *171*, 115381. [CrossRef] [PubMed]
6. Chow, S.J.; Croll, H.C.; Ojeda, N.; Klamerus, J.; Capelle, R.; Oppenheimer, J.; Jacangelo, J.G.; Schwab, K.J.; Prasse, C. Comparative investigation of PFAS adsorption onto activated carbon and anion exchange resins during long-term operation of a pilot treatment plant. *Water Res.* **2022**, *226*, 119198. [CrossRef]
7. Bolan, N.; Sarkar, B.; Vithanage, M.; Singh, G.; Tsang, D.C.W.; Mukhopadhyay, R.; Ramadass, K.; Vinu, A.; Sun, Y.; Ramanayaka, S.; et al. Distribution, behaviour, bioavailability and remediation of poly- and per-fluoroalkyl substances (PFAS) in solid biowastes and biowaste-treated soil. *Environ. Int.* **2021**, *155*, 106600. [CrossRef]
8. Bruton, T.K.; Sedlak, D.L. Treatment of Aqueous Film-Forming Foam by Heat-Activated Persulfate Under Conditions Representative of In Situ Chemical Oxidation. *Environ. Sci. Technol.* **2017**, *51*, 13878–13885. [CrossRef]
9. Bao, Y.; Huang, J.; Cagnetta, G.; Yu, G. Removal of F-538 as PFOS alternative in chrome plating wastewater by UV/Sulfite reduction. *Water Res.* **2019**, *163*, 114907. [CrossRef]
10. Cui, J.; Gao, P.; Deng, Y. Destruction of Per- and Polyfluoroalkyl Substances (PFAS) with Advanced Reduction Processes (ARPs): A Critical Review. *Environ. Sci. Technol.* **2020**, *54*, 3752–3766. [CrossRef]
11. Pierpaoli, M.; Szopińska, M.; Wilk, B.K.; Sobaszek, M.; Łuczkiewicz, A.; Bogdanowicz, R.; Fudala-Książek, S. Electrochemical oxidation of PFOA and PFOS in landfill leachates at low and highly boron-doped diamond electrodes. *J. Hazard. Mater.* **2021**, *403*, 123606. [CrossRef]
12. Wackett, L.P. Why Is the Biodegradation of Polyfluorinated Compounds So Rare? *mSphere* **2021**, *6*, 10–1128. [CrossRef]

13. Glaze, W.H.; Kang, J.-W.; Chapin, D.H. The Chemistry of Water Treatment Processes Involving Ozone, Hydrogen Peroxide and Ultraviolet Radiation. *Ozone Sci. Eng.* **1987**, *9*, 335–352. [CrossRef]
14. Yang, L.; Jiao, Y.; Xu, X.; Pan, Y.; Su, C.; Duan, X.; Sun, H.; Liu, S.; Wang, S.; Shao, Z. Superstructures with Atomic-Level Arranged Perovskite and Oxide Layers for Advanced Oxidation with an Enhanced Non-Free Radical Pathway. *ACS Sustain. Chem. Eng.* **2022**, *10*, 1899–1909. [CrossRef]
15. Leonello, D.; Fendrich, M.A.; Parrino, F.; Patel, N.; Orlandi, M.; Miotello, A. Light-Induced Advanced Oxidation Processes as PFAS Remediation Methods: A Review. *Appl. Sci.* **2021**, *11*, 8468. [CrossRef]
16. Broman, J.; Ceja, A.; Godoy, T.; Rivera, D.R.; Dionne, P.; Schipper, J.; Henkemeyer, S.; Cegielski, S.; Wong, G.; Kaur, A.; et al. Destruction of Per- and Polyfluoroalkyl Substances (PFAS) via Lacasse Enzymatic Degradation and Electrochemical Advanced Oxidation. In Proceedings of the 31st Waste-Management Education Research Conference (WERC), Las Cruces, NM, USA, 11–14 April 2021.
17. Xiao, F.; Sasi, P.C.; Alinezhad, A.; Sun, R.; Ali, M.A. Thermal Phase Transition and Rapid Degradation of Forever Chemicals (PFAS) in Spent Media Using Induction Heating. *ACS ES&T Eng.* **2023**, *3*, 1370–1380.
18. Horikoshi, S.; Sato, S.; Abe, M.; Serpone, N. A novel liquid plasma AOP device integrating microwaves and ultrasounds and its evaluation in defluorinating perfluorooctanoic acid in aqueous media. *Ultrason. Sonochem.* **2011**, *18*, 938–942. [CrossRef]
19. Ma, Q.; Gao, J.; Moussa, B.; Young, J.; Zhao, M.; Zhang, W. Electrosorption, Desorption, and Oxidation of Perfluoroalkyl Carboxylic Acids (PFCAs) via MXene-Based Electrocatalytic Membranes. *ACS Appl. Mater. Interfaces* **2023**, *15*, 29149–29159. [CrossRef]
20. Han, J.; Zhao, M.; Wu, K.; Hong, Y.; Huang, T.; Gu, X.; Wang, Z.; Liu, S.; Zhu, G. A bifunctional single-atom catalyst assisted by Fe2O3 for efficiently electrocatalytic perfluorooctanoic acid degradation by integrating reductive and oxidative processes. *Chem. Eng. J.* **2023**, *470*, 144270. [CrossRef]
21. Wang, C.; Zhang, T.; Yin, L.; Ni, C.; Ni, J.; Hou, L.-A. Enhanced perfluorooctane acid mineralization by electrochemical oxidation using Ti_3+ self-doping TiO_2 nanotube arrays anode. *Chemosphere* **2022**, *286*, 131804. [CrossRef]
22. Lou, Z.; Wang, J.; Wang, S.; Xu, Y.; Wang, J.; Liu, B.; Yu, C.; Yu, J. Strong hydrophobic affinity and enhanced •OH generation boost energy-efficient electrochemical destruction of perfluorooctanoic acid on robust ceramic/PbO2-PTFE anode. *Sep. Purif. Technol.* **2022**, *280*, 119919. [CrossRef]
23. Mojiri, A.; Zhou, J.L.; Ozaki, N.; KarimiDermani, B.; Razmi, E.; Kasmuri, N. Occurrence of per- and polyfluoroalkyl substances in aquatic environments and their removal by advanced oxidation processes. *Chemosphere* **2023**, *330*, 138666. [CrossRef]
24. Chowdhury, N.; Choi, H. Photocatalytic degradation of perfluorooctanoic acid on Pb-doped TiO_2 coated with reduced graphene oxide. *Water Environ. Res.* **2023**, *95*, e10871. [CrossRef] [PubMed]
25. McQueen, A.D.; Tedrow, O.N.; Ballentine, M.L.; Kennedy, A.J. Demonstration of Photocatalytic Degradation of Per- and Polyfluoroalkyl Substances (PFAS) in Landfill Leachate Using 3D Printed TiO_2 Composite Tiles. *Water Air Soil Pollut.* **2022**, *233*, 444. [CrossRef]
26. Liu, X.; Duan, X.; Bao, T.; Hao, D.; Chen, Z.; Wei, W.; Wang, D.; Wang, S.; Ni, B.-J. High-performance photocatalytic decomposition of PFOA by BiOX/TiO_2 heterojunctions: Self-induced inner electric fields and band alignment. *J. Hazard. Mater.* **2022**, *430*, 128195. [CrossRef] [PubMed]
27. Fu, C.; Xu, X.; Zheng, C.; Liu, X.; Zhao, D.; Qiu, W. Photocatalysis of aqueous PFOA by common catalysts of In_2O_3, Ga_2O_3, TiO_2, CeO_2 and CdS: Influence factors and mechanistic insights. *Environ. Geochem. Health* **2022**, *44*, 2943–2953. [CrossRef] [PubMed]
28. Duan, L.; Wang, B.; Heck, K.N.; Clark, C.A.; Wei, J.; Wang, M.; Metz, J.; Wu, G.; Tsai, A.-L.; Guo, S.; et al. Titanium oxide improves boron nitride photocatalytic degradation of perfluorooctanoic acid. *Chem. Eng. J.* **2022**, *448*, 137735. [CrossRef]
29. Li, F.; Duan, J.; Tian, S.; Ji, H.; Zhu, Y.; Wei, Z.; Zhao, D. Short-chain per- and polyfluoroalkyl substances in aquatic systems: Occurrence, impacts and treatment. *Chem. Eng. J.* **2020**, *380*, 122506. [CrossRef]
30. Lu, D.; Sha, S.; Luo, J.; Huang, Z.; Zhang Jackie, X. Treatment train approaches for the remediation of per- and polyfluoroalkyl substances (PFAS): A critical review. *J. Hazard. Mater.* **2020**, *386*, 121963. [CrossRef]
31. Verma, S.; Varma, R.S.; Nadagouda, M.N. Remediation and mineralization processes for per- and polyfluoroalkyl substances (PFAS) in water: A review. *Sci. Total Environ.* **2021**, *794*, 148987. [CrossRef]
32. Banks, D.; Jun, B.-M.; Heo, J.; Her, N.; Park, C.M.; Yoon, Y. Selected advanced water treatment technologies for perfluoroalkyl and polyfluoroalkyl substances: A review. *Sep. Purif. Technol.* **2020**, *231*, 115929. [CrossRef]
33. Nzeribe, N.; Crimi, M.; Thagard, S.M.; Holsen, T.M. Physico-Chemical Processes for the Treatment of Per- And Polyfluoroalkyl Substances (PFAS): A review Blossom. *Crit. Rev. Environ. Sci. Technol.* **2019**, *49*, 866–915. [CrossRef]
34. Trojanowicz, M.; Bojanowska-Czajka, A.; Bartosiewicz, I.; Kulisa, K. Advanced Oxidation/Reduction Processes treatment for aqueous perfluorooctanoate (PFOA) and perfluorooctanesulfonate (PFOS)—A review of recent advances. *Chem. Eng. J.* **2018**, *336*, 170–199. [CrossRef]
35. Gar Alalm, M.; Boffito, D.C. Mechanisms and pathways of PFAS degradation by advanced oxidation and reduction processes: A critical review. *Chem. Eng. J.* **2022**, *450*, 138352. [CrossRef]
36. Wang, J.; Wang, S. Reactive species in advanced oxidation processes: Formation, identification and reaction mechanism. *Chem. Eng. J.* **2020**, *401*, 126158. [CrossRef]
37. Yu, G.; Wang, Y.; Cao, H.; Zhao, H.; Xie, Y. Reactive Oxygen Species and Catalytic Active Sites in Heterogeneous Catalytic Ozonation for Water Purification. *Environ. Sci. Technol.* **2020**, *54*, 5931–5946. [CrossRef]

38. Xu, B.; Zhou, J.L.; Altaee, A.; Ahmed, M.B.; Johir, M.A.H.; Ren, J.; Li, X. Improved photocatalysis of perfluorooctanoic acid in water and wastewater by Ga_2O_3/UV system assisted by peroxymonosulfate. *Chemosphere* **2020**, *239*, 124722. [CrossRef]
39. Wang, J.; Cao, C.; Zhang, Y.; Zhang, Y.; Zhu, L. Underneath mechanisms into the super effective degradation of PFOA by BiOF nanosheets with tunable oxygen vacancies on exposed (101) facets. *Appl. Catal. B* **2021**, *286*, 119911. [CrossRef]
40. Samy, M.; Ibrahim, M.G.; Fujii, M.; Diab, K.E.; ElKady, M.; Gar Alalm, M. CNTs/MOF-808 painted plates for extended treatment of pharmaceutical and agrochemical wastewaters in a novel photocatalytic reactor. *Chem. Eng. J.* **2021**, *406*, 127152. [CrossRef]
41. Cao, M.H.; Wang, B.B.; Yu, H.S.; Wang, L.L.; Yuan, S.H.; Chen, J. Photochemical decomposition of perfluorooctanoic acid in aqueous periodate with VUV and UV light irradiation. *J. Hazard. Mater.* **2010**, *179*, 1143–1146. [CrossRef]
42. Li, Z.; Zhang, P.; Shao, T.; Li, X. In_2O_3 nanoporous nanosphere: A highly efficient photocatalyst for decomposition of perfluorooctanoic acid. *Appl. Catal. B* **2012**, *125*, 350–357. [CrossRef]
43. Liu, X.; Wei, W.; Xu, J.; Wang, D.; Song, L.; Ni, B.-J. Photochemical decomposition of perfluorochemicals in contaminated water. *Water Res.* **2020**, *186*, 116311. [CrossRef]
44. Song, Z.; Tang, H.; Wang, N.; Zhu, L. Reductive defluorination of perfluorooctanoic acid by hydrated electrons in a sulfite-mediated UV photochemical system. *J. Hazard. Mater.* **2013**, *262*, 332–338. [CrossRef]
45. Bentel, M.J.; Yu, Y.; Xu, L.; Li, Z.; Wong, B.M.; Men, Y.; Liu, J. Defluorination of Per- and Polyfluoroalkyl Substances (PFASs) with Hydrated Electrons: Structural Dependence and Implications to PFAS Remediation and Management. *Environ. Sci. Technol.* **2019**, *53*, 3718–3728. [CrossRef]
46. Li, X.; Zhang, P.; Jin, L.; Shao, T.; Li, Z.; Cao, J. Efficient Photocatalytic Decomposition of Perfluorooctanoic Acid by Indium Oxide and Its Mechanism. *Environ. Sci. Technol.* **2012**, *46*, 5528–5534. [CrossRef] [PubMed]
47. Banayan Esfahani, E.; Asadi Zeidabadi, F.; Zhang, S.; Mohseni, M. Photo-chemical/catalytic oxidative/reductive decomposition of per- and poly-fluoroalkyl substances (PFAS), decomposition mechanisms and effects of key factors: A review. *Environ. Sci. Water Res. Technol.* **2022**, *8*, 698–728. [CrossRef]
48. Eberson, L. Electron-Transfer Reactions in Organic Chemistry. *Adv. Phys. Org. Chem.* **1982**, *18*, 79–185.
49. Zhang, H.; Xie, C.; Chen, L.; Duan, J.; Li, F.; Liu, W. Different reaction mechanisms of SO_4•− and •OH with organic compound interpreted at molecular orbital level in Co(II)/peroxymonosulfate catalytic activation system. *Water Res.* **2023**, *229*, 119392. [CrossRef]
50. Wang, J.; Wang, S. Activation of persulfate (PS) and peroxymonosulfate (PMS) and application for the degradation of emerging contaminants. *Chem. Eng. J.* **2018**, *334*, 1502–1517. [CrossRef]
51. Moreira, F.C.; Boaventura, R.A.R.; Brillas, E.; Vilar, V.J.P. Electrochemical advanced oxidation processes: A review on their application to synthetic and real wastewaters. *Appl. Catal. B* **2017**, *202*, 217–261. [CrossRef]
52. Yadav, S.; Ibrar, I.; Al-Juboori, R.A.; Singh, L.; Ganbat, N.; Kazwini, T.; Karbassiyazdi, E.; Samal, A.K.; Subbiah, S.; Altaee, A. Updated review on emerging technologies for PFAS contaminated water treatment. *Chem. Eng. Res. Des.* **2022**, *182*, 667–700. [CrossRef]
53. Wang, Y.; Zhang, P. Effects of pH on photochemical decomposition of perfluorooctanoic acid in different atmospheres by 185nm vacuum ultraviolet. *J. Environ. Sci.* **2014**, *26*, 2207–2214. [CrossRef] [PubMed]
54. Giri, R.R.; Ozaki, H.; Okada, T.; Taniguchi, S.; Takanami, R. Factors influencing UV photodecomposition of perfluorooctanoic acid in water. *Chem. Eng. J.* **2012**, *180*, 197–203. [CrossRef]
55. Wang, S.; Yang, Q.; Chen, F.; Sun, J.; Luo, K.; Yao, F.; Wang, X.; Wang, D.; Li, X.; Zeng, G. Photocatalytic degradation of perfluorooctanoic acid and perfluorooctane sulfonate in water: A critical review. *Chem. Eng. J.* **2017**, *328*, 927–942. [CrossRef]
56. Phan Thi, L.-A.; Do, H.-T.; Lee, Y.-C.; Lo, S.-L. Photochemical decomposition of perfluorooctanoic acids in aqueous carbonate solution with UV irradiation. *Chem. Eng. J.* **2013**, *221*, 258–263. [CrossRef]
57. Qanbarzadeh, M.; Wang, D.; Ateia, M.; Sahu, S.P.; Cates, E.L. Impacts of Reactor Configuration, Degradation Mechanisms, and Water Matrices on Perfluorocarboxylic Acid Treatment Efficiency by the UV/$Bi_3O(OH)(PO_4)_2$ Photocatalytic Process. *ACS ES&T Eng.* **2021**, *1*, 239–248.
58. Samy, M.; Ibrahim, M.G.; Gar Alalm, M.; Fujii, M. MIL-53(Al)/ZnO coated plates with high photocatalytic activity for extended degradation of trimethoprim via novel photocatalytic reactor. *Sep. Purif. Technol.* **2020**, *249*, 117173. [CrossRef]
59. Fouad, M.; Gar Alalm, M.; El-Etriby, H.K.; Boffito, D.C.; Ookawara, S.; Ohno, T.; Fujii, M. Visible-light-driven photocatalytic disinfection of raw surface waters (300–5000 CFU/mL) using reusable coated Ru/WO_3/ZrO_2. *J. Hazard. Mater.* **2021**, *402*, 123514. [CrossRef] [PubMed]
60. Hossain, M.S.; Mollah, M.Y.A.; Susan, M.A.B.H.; Islam, M.M. Role of in situ electrogenerated reactive oxygen species towards degradation of organic dye in aqueous solution. *Electrochim. Acta* **2020**, *344*, 136146. [CrossRef]
61. Liu, X.Y.; Zhang, Y.Q.; Xia, X.H.; Shi, S.J.; Lu, Y.; Wang, X.L.; Gu, C.D.; Tu, J.P. Self-assembled porous $NiCo_2O_4$ hetero-structure array for electrochemical capacitor. *J. Power Sour.* **2013**, *239*, 157–163. [CrossRef]
62. Panizza, M.; Cerisola, G. Direct and Mediated Anodic Oxidation of Organic Pollutants. *Chem. Rev.* **2009**, *109*, 6541–6569. [CrossRef]
63. Lin, H.; Niu, J.; Ding, S.; Zhang, L. Electrochemical degradation of perfluorooctanoic acid (PFOA) by Ti/SnO_2–Sb, Ti/SnO_2–Sb/PbO_2 and Ti/SnO_2–Sb/MnO_2 anodes. *Water Res.* **2012**, *46*, 2281–2289. [CrossRef]
64. Niu, J.; Lin, H.; Gong, C.; Sun, X. Theoretical and Experimental Insights into the Electrochemical Mineralization Mechanism of Perfluorooctanoic Acid. *Environ. Sci. Technol.* **2013**, *47*, 14341–14349. [CrossRef]

65. Zhuo, Q.; Deng, S.; Yang, B.; Huang, J.; Yu, G. Efficient Electrochemical Oxidation of Perfluorooctanoate Using a Ti/SnO_2-Sb-Bi Anode. *Environ. Sci. Technol.* **2011**, *45*, 2973–2979. [CrossRef] [PubMed]
66. Lin, H.; Niu, J.; Xu, J.; Huang, H.; Li, D.; Yue, Z.; Feng, C. Highly Efficient and Mild Electrochemical Mineralization of Long-Chain Perfluorocarboxylic Acids (C9–C10) by Ti/SnO_2–Sb–Ce, Ti/SnO_2–Sb/Ce–PbO_2, and Ti/BDD Electrodes. *Environ. Sci. Technol.* **2013**, *47*, 13039–13046. [CrossRef] [PubMed]
67. Niu, J.; Lin, H.; Xu, J.; Wu, H.; Li, Y. Electrochemical Mineralization of Perfluorocarboxylic Acids (PFCAs) by Ce-Doped Modified Porous Nanocrystalline PbO_2 Film Electrode. *Environ. Sci. Technol.* **2012**, *46*, 10191–10198. [CrossRef]
68. Ma, Q.; Liu, L.; Cui, W.; Li, R.; Song, T.; Cui, Z. Electrochemical degradation of perfluorooctanoic acid (PFOA) by Yb-doped Ti/SnO_2–Sb/PbO_2 anodes and determination of the optimal conditions. *RSC Adv.* **2015**, *5*, 84856–84864. [CrossRef]
69. Wang, K.; Huang, D.; Wang, W.; Ji, Y.; Niu, J. Enhanced perfluorooctanoic acid degradation by electrochemical activation of peroxymonosulfate in aqueous solution. *Environ. Int.* **2020**, *137*, 105562. [CrossRef]
70. Estrellan, C.R.; Salim, C.; Hinode, H. Photocatalytic decomposition of perfluorooctanoic acid by iron and niobium co-doped titanium dioxide. *J. Hazard. Mater.* **2010**, *179*, 79–83. [CrossRef]
71. Yao, X.; Zuo, J.; Wang, Y.-J.; Song, N.-N.; Li, H.-H.; Qiu, K. Enhanced Photocatalytic Degradation of Perfluorooctanoic Acid by Mesoporous Sb_2O_3/TiO_2 Heterojunctions. *Front. Chem.* **2021**, *9*, 690520. [CrossRef]
72. Ryou, H.; Yoo, T.H.; Yoon, Y.; Lee, I.G.; Shin, M.; Cho, J.; Cho, B.J.; Hwang, W.S. Hydrothermal Synthesis and Photocatalytic Property of Sn-doped β-Ga_2O_3 Nanostructure. *ECS J. Solid State Sci. Technol.* **2020**, *9*, 045009. [CrossRef]
73. Wang, J.; Cao, C.; Wang, Y.; Wang, Y.; Sun, B.; Zhu, L. In situ preparation of p-n BiOI@Bi5O7I heterojunction for enhanced PFOA photocatalytic degradation under simulated solar light irradiation. *Chem. Eng. J.* **2020**, *391*, 123530. [CrossRef]
74. Wu, Y.; Li, Y.; Fang, C.; Li, C. Highly Efficient Degradation of Perfluorooctanoic Acid over a MnOx-Modified Oxygen-Vacancy-Rich In_2O_3 Photocatalyst. *ChemCatChem* **2019**, *11*, 2297–2303. [CrossRef]
75. Xu, B.; Ahmed, M.B.; Zhou, J.L.; Altaee, A. Visible and UV photocatalysis of aqueous perfluorooctanoic acid by TiO_2 and peroxymonosulfate: Process kinetics and mechanistic insights. *Chemosphere* **2020**, *243*, 125366. [CrossRef] [PubMed]
76. Chen, M.-J.; Lo, S.-L.; Lee, Y.-C.; Kuo, J.; Wu, C.-H. Decomposition of perfluorooctanoic acid by ultraviolet light irradiation with Pb-modified titanium dioxide. *J. Hazard. Mater.* **2016**, *303*, 111–118. [CrossRef] [PubMed]
77. Zhao, B.; Li, X.; Yang, L.; Wang, F.; Li, J.; Xia, W.; Li, W.; Zhou, L.; Zhao, C. ß-Ga_2O_3 Nanorod Synthesis with a One-step Microwave Irradiation Hydrothermal Method and its Efficient Photocatalytic Degradation for Perfluorooctanoic Acid. *Photochem. Photobiol.* **2015**, *91*, 42–47. [CrossRef] [PubMed]
78. Fujishima, A.; Honda, K. Electrochemical Photolysis of Water at a Semiconductor Electrode. *Nature* **1972**, *238*, 37–38. [CrossRef]
79. Chen, M.-J.; Lo, S.-L.; Lee, Y.-C.; Huang, C.-C. Photocatalytic decomposition of perfluorooctanoic acid by transition-metal modified titanium dioxide. *J. Hazard. Mater.* **2015**, *288*, 168–175. [CrossRef]
80. Li, M.; Yu, Z.; Liu, Q.; Sun, L.; Huang, W. Photocatalytic decomposition of perfluorooctanoic acid by noble metallic nanoparticles modified TiO_2. *Chem. Eng. J.* **2016**, *286*, 232–238. [CrossRef]
81. Liu, Q.; Yu, Z.-b.; Zhang, R.-h.; Li, M.-j.; Chen, Y.; Wang, L.; Kuang, Y.; Zhang, B.; Zhu, Y.-h. Photocatalytic Degradation of Perfluorooctanoic Acid by Pd-TiO2 Photocatalyst. *Huanjing Kexue* **2015**, *36*, 2138–2146.
82. Tian, A.; Wu, Y.; Mao, K. Enhanced Performance of Surface Modified TiO_2 Nanotubes for the Decomposition of Perfluorooctanoic Acid. In Proceedings of the International Conference on Materials Science, Resource and Environmental Engineering (MSREE), Xian, China, 10–11 December 2016.
83. Peng, Y.-P.; Chen, H.; Huang, C.P. The Synergistic Effect of Photoelectrochemical (PEC) Reactions Exemplified by Concurrent Perfluorooctanoic acid (PFOA) Degradation and Hydrogen Generation over Carbon and Nitrogen codoped TiO_2 Nanotube Arrays (C-N-TNTAs) photoelectrode. *Appl. Catal. B-Environ.* **2017**, *209*, 437–446. [CrossRef]
84. Song, C.; Chen, P.; Wang, C.; Zhu, L. Photodegradation of perfluorooctanoic acid by synthesized TiO_2–MWCNT composites under 365 nm UV irradiation. *Chemosphere* **2012**, *86*, 853–859. [CrossRef]
85. Wang, Y.; Wang, C.; Luo, P.; Hu, Q. Removal of perfluorooctanoic acid by MWCNT-modified carbon-doped titanium dioxide in a peroxymonosulfate/simulated sunlight system. *Appl. Surf. Sci.* **2023**, *614*, 156251. [CrossRef]
86. Panchangam, S.C.; Yellatur, C.S.; Yang, J.-S.; Loka, S.S.; Lin, A.Y.C.; Vemula, V. Facile fabrication of TiO_2-graphene nanocomposites (TGNCs) for the efficient photocatalytic oxidation of perfluorooctanoic acid (PFOA). *J. Environ. Chem. Eng.* **2018**, *6*, 6359–6369. [CrossRef]
87. Yang, J.-S.; Lai, W.W.-P.; Panchangam, S.C.; Lin, A.Y.-C. Photoelectrochemical degradation of perfluorooctanoic acid (PFOA) with GOP25/FTO anodes: Intermediates and reaction pathways. *J. Hazard. Mater.* **2020**, *391*, 122247. [CrossRef] [PubMed]
88. Zhu, C.; Xu, J.; Song, S.; Wang, J.; Li, Y.; Liu, R.; Shen, Y. TiO_2 quantum dots loaded sulfonated graphene aerogel for effective adsorption-photocatalysis of PFOA. *Sci. Total Environ.* **2020**, *698*, 134275. [CrossRef]
89. Gomez-Ruiz, B.; Ribao, P.; Diban, N.; Rivero, M.J.; Ortiz, I.; Urtiaga, A. Photocatalytic degradation and mineralization of perfluorooctanoic acid (PFOA) using a composite TiO_2 −rGO catalyst. *J. Hazard. Mater.* **2018**, *344*, 950–957. [CrossRef]
90. Li, F.; Wei, Z.; He, K.; Blaney, L.; Cheng, X.; Xu, T.; Liu, W.; Zhao, D. A concentrate-and-destroy technique for degradation of perfluorooctanoic acid in water using a new adsorptive photocatalyst. *Water Res.* **2020**, *185*, 116219. [CrossRef]
91. Li, Z.; Zhang, P.; Shao, T.; Wang, J.; Jin, L.; Li, X. Different nanostructured In_2O_3 for photocatalytic decomposition of perfluorooctanoic acid (PFOA). *J. Hazard. Mater.* **2013**, *260*, 40–46. [CrossRef]

92. Li, Z.; Zhang, P.; Li, J.; Shao, T.; Wang, J.; Jin, L. Synthesis of In_2O_3 porous nanoplates for photocatalytic decomposition of perfluorooctanoic acid (PFOA). *Catal. Commun.* **2014**, *43*, 42–46. [CrossRef]
93. Xu, C.; Qiu, P.; Chen, H.; Jiang, F.; Wang, X. Fabrication of two-dimensional indium oxide nanosheets with graphitic carbon nitride nanosheets as sacrificial templates. *Mater. Lett.* **2019**, *242*, 24–27. [CrossRef]
94. Jiang, F.; Zhao, H.; Chen, H.; Xu, C.; Chen, J. Enhancement of photocatalytic decomposition of perfluorooctanoic acid on CeO_2/In_2O_3. *RSC Adv.* **2016**, *6*, 72015–72021. [CrossRef]
95. Tan, X.; Chen, G.; Xing, D.; Ding, W.; Liu, H.; Li, T.; Huang, Y. Indium-modified Ga_2O_3 hierarchical nanosheets as efficient photocatalysts for the degradation of perfluorooctanoic acid. *Environ. Sci. Nano* **2020**, *7*, 2229–2239. [CrossRef]
96. Li, Y.; Wang, J.; Yao, H.; Dang, L.; Li, Z. Efficient decomposition of organic compounds and reaction mechanism with BiOI photocatalyst under visible light irradiation. *J. Mol. Catal. A Chem.* **2011**, *334*, 116–122. [CrossRef]
97. Li, T.; Wang, C.; Wang, T.; Zhu, L. Highly efficient photocatalytic degradation toward perfluorooctanoic acid by bromine doped BiOI with high exposure of (001) facet. *Appl. Catal. B* **2020**, *268*, 118442. [CrossRef]
98. Zhang, K.-L.; Liu, C.-M.; Huang, F.-Q.; Zheng, C.; Wang, W.-D. Study of the electronic structure and photocatalytic activity of the BiOCl photocatalyst. *Appl. Catal. B* **2006**, *68*, 125–129. [CrossRef]
99. Song, Z.; Dong, X.; Wang, N.; Zhu, L.; Luo, Z.; Fang, J.; Xiong, C. Efficient photocatalytic defluorination of perfluorooctanoic acid over BiOCl nanosheets via a hole direct oxidation mechanism. *Chem. Eng. J.* **2017**, *317*, 925–934. [CrossRef]
100. Sun, Y.; Li, G.; Wang, W.; Gu, W.; Wong, P.K.; An, T. Photocatalytic defluorination of perfluorooctanoic acid by surface defective BiOCl: Fast microwave solvothermal synthesis and photocatalytic mechanisms. *J. Environ. Sci.* **2019**, *84*, 69–79. [CrossRef] [PubMed]
101. Yang, Y.; Zheng, Z.; Yang, M.; Chen, J.; Li, C.; Zhang, C.; Zhang, X. In-situ fabrication of a spherical-shaped Zn-Al hydrotalcite with BiOCl and study on its enhanced photocatalytic mechanism for perfluorooctanoic acid removal performed with a response surface methodology. *J. Hazard. Mater.* **2020**, *399*, 123070. [CrossRef]
102. Sahu, S.P.; Qanbarzadeh, M.; Ateia, M.; Torkzadeh, H.; Maroli, A.S.; Cates, E.L. Rapid Degradation and Mineralization of Perfluorooctanoic Acid by a New Petitjeanite $Bi_3O(OH)(PO_4)_2$ Microparticle Ultraviolet Photocatalyst. *Environ. Sci. Technol. Lett.* **2018**, *5*, 533–538. [CrossRef]
103. Xu, T.; Zhu, Y.; Duan, J.; Xia, Y.; Tong, T.; Zhang, L.; Zhao, D. Enhanced photocatalytic degradation of perfluorooctanoic acid using carbon-modified bismuth phosphate composite: Effectiveness, material synergy and roles of carbon. *Chem. Eng. J.* **2020**, *395*, 124991. [CrossRef]
104. Huang, G.; Zhang, G.; Gao, Z.; Cao, J.; Li, D.; Yun, H.; Zeng, T. Enhanced visible-light-driven photocatalytic activity of BiFeO3 via electric-field control of spontaneous polarization. *J. Alloys Compd.* **2019**, *783*, 943–951. [CrossRef]
105. Li, S.; Zhang, G.; Zhang, W.; Zheng, H.; Zhu, W.; Sun, N.; Zheng, Y.; Wang, P. Microwave enhanced Fenton-like process for degradation of perfluorooctanoic acid (PFOA) using Pb-$BiFeO_3$/rGO as heterogeneous catalyst. *Chem. Eng. J.* **2017**, *326*, 756–764. [CrossRef]
106. Shang, E.; Li, Y.; Niu, J.; Li, S.; Zhang, G.; Wang, X. Photocatalytic degradation of perfluorooctanoic acid over Pb-$BiFeO_3$/rGO catalyst: Kinetics and mechanism. *Chemosphere* **2018**, *211*, 34–43. [CrossRef] [PubMed]
107. Qian, L.; Georgi, A.; Gonzalez-Olmos, R.; Kopinke, F.-D. Degradation of perfluorooctanoic acid adsorbed on Fe-zeolites with molecular oxygen as oxidant under UV-A irradiation. *Appl. Catal. B Environ.* **2020**, *278*, 119283. [CrossRef]
108. Luo, D.; Yuan, J.; Zhou, J.; Zou, M.; Xi, R.; Qin, Y.; Shen, Q.; Hu, S.; Xu, J.; Nie, M.; et al. Synthesis of samarium doped ferrite and its enhanced photocatalytic degradation of perfluorooctanoic acid (PFOA). *Opt. Mater.* **2021**, *122*, 111636. [CrossRef]
109. Xu, J.; Wu, M.; Yang, J.; Wang, Z.; Chen, M.; Teng, F. Efficient photocatalytic degradation of perfluorooctanoic acid by a wide band gap p-block metal oxyhydroxide InOOH. *Appl. Surf. Sci.* **2017**, *416*, 587–592. [CrossRef]
110. Zhao, H.; Gao, J.; Zhao, G.; Fan, J.; Wang, Y.; Wang, Y. Fabrication of novel SnO_2-Sb/carbon aerogel electrode for ultrasonic electrochemical oxidation of perfluorooctanoate with high catalytic efficiency. *Appl. Catal. B* **2013**, *136–137*, 278–286. [CrossRef]
111. Duan, L.; Wang, B.; Heck, K.; Guo, S.; Clark, C.A.; Arredondo, J.; Wang, M.; Senftle, T.P.; Westerhoff, P.; Wen, X.; et al. Efficient Photocatalytic PFOA Degradation over Boron Nitride. *Environ. Sci. Technol. Lett.* **2020**, *7*, 613–619. [CrossRef]
112. Zhu, Y.; Xu, T.; Zhao, D.; Li, F.; Liu, W.; Wang, B.; An, B. Adsorption and solid-phase photocatalytic degradation of perfluorooctane sulfonate in water using gallium-doped carbon-modified titanate nanotubes. *Chem. Eng. J.* **2021**, *421*, 129676. [CrossRef]
113. Chen, Y.-C.; Lo, S.-L.; Kuo, J. Effects of titanate nanotubes synthesized by a microwave hydrothermal method on photocatalytic decomposition of perfluorooctanoic acid. *Water Res.* **2011**, *45*, 4131–4140. [CrossRef]
114. Song, H.; Wang, Y.; Ling, Z.; Zu, D.; Li, Z.; Shen, Y.; Li, C. Enhanced photocatalytic degradation of perfluorooctanoic acid by Ti_3C_2 MXene-derived heterojunction photocatalyst: Application of intercalation strategy in DESs. *Sci. Total Environ.* **2020**, *746*, 141009. [CrossRef]
115. Li, Z.; Zhang, P.; Li, J.; Shao, T.; Jin, L. Synthesis of In_2O_3-graphene composites and their photocatalytic performance towards perfluorooctanoic acid decomposition. *J. Photochem. Photobiol. A Chem.* **2013**, *271*, 111–116. [CrossRef]
116. Xu, C.; Qiu, P.; Chen, H.; Jiang, F. Platinum modified indium oxide nanorods with enhanced photocatalytic activity on degradation of perfluorooctanoic acid (PFOA). *J. Taiwan Inst. Chem. Eng.* **2017**, *80*, 761–768. [CrossRef]
117. Wu, D.; Li, X.; Tang, Y.; Lu, P.; Chen, W.; Xu, X.; Li, L. Mechanism insight of PFOA degradation by ZnO assisted-photocatalytic ozonation: Efficiency and intermediates. *Chemosphere* **2017**, *180*, 247–252. [CrossRef] [PubMed]

118. Wu, D.; Li, X.; Zhang, J.; Chen, W.; Lu, P.; Tang, Y.; Li, L. Efficient PFOA degradation by persulfate-assisted photocatalytic ozonation. *Sep. Purif. Technol.* **2018**, *207*, 255–261. [CrossRef]
119. Bacha, A.-U.-R.; Nabi, I.; Fu, Z.; Li, K.; Cheng, H.; Zhang, L. A comparative study of bismuth-based photocatalysts with titanium dioxide for perfluorooctanoic acid degradation. *Chin. Chem. Lett.* **2019**, *30*, 2225–2230. [CrossRef]
120. Liu, Y.; Fan, X.; Quan, X.; Fan, Y.; Chen, S.; Zhao, X. Enhanced Perfluorooctanoic Acid Degradation by Electrochemical Activation of Sulfate Solution on B/N Codoped Diamond. *Environ. Sci. Technol.* **2019**, *53*, 5195–5201. [CrossRef]
121. Lin, H.; Xiao, R.; Xie, R.; Yang, L.; Tang, C.; Wang, R.; Chen, J.; Lv, S.; Huang, Q. Defect Engineering on a Ti_4O_7 Electrode by Ce_3+ Doping for the Efficient Electrooxidation of Perfluorooctanesulfonate. *Environ. Sci. Technol.* **2021**, *55*, 2597–2607. [CrossRef]
122. Yang, B.; Jiang, C.; Yu, G.; Zhuo, Q.; Deng, S.; Wu, J.; Zhang, H. Highly efficient electrochemical degradation of perfluorooctanoic acid (PFOA) by F-doped Ti/SnO2 electrode. *J. Hazard. Mater.* **2015**, *299*, 417–424. [CrossRef]
123. Sukeesan, S.; Boontanon, N.; Boontanon, S.K. Improved electrical driving current of electrochemical treatment of Per- and Polyfluoroalkyl Substances (PFAS) in water using Boron-Doped Diamond anode. *Environ. Technol. Innov.* **2021**, *23*, 101655. [CrossRef]
124. Song, S.; Zhan, L.; He, Z.; Lin, L.; Tu, J.; Zhang, Z.; Chen, J.; Xu, L. Mechanism of the anodic oxidation of 4-chloro-3-methyl phenol in aqueous solution using Ti/SnO_2–Sb/PbO_2 electrodes. *J. Hazard. Mater.* **2010**, *175*, 614–621. [CrossRef]
125. Duan, T.; Wen, Q.; Chen, Y.; Zhou, Y.; Duan, Y. Enhancing electrocatalytic performance of Sb-doped SnO2 electrode by compositing nitrogen-doped graphene nanosheets. *J. Hazard. Mater.* **2014**, *280*, 304–314. [CrossRef] [PubMed]
126. Ochiai, T.; Iizuka, Y.; Nakata, K.; Murakami, T.; Tryk, D.A.; Fujishima, A.; Koide, Y.; Morito, Y. Efficient electrochemical decomposition of perfluorocarboxylic acids by the use of a boron-doped diamond electrode. *Diamond Relat. Mater.* **2011**, *20*, 64–67. [CrossRef]
127. Carter, K.E.; Farrell, J. Oxidative Destruction of Perfluorooctane Sulfonate Using Boron-Doped Diamond Film Electrodes. *Environ. Sci. Technol.* **2008**, *42*, 6111–6115. [CrossRef]
128. Zhi, J.-F.; Wang, H.-B.; Nakashima, T.; Rao, T.N.; Fujishima, A. Electrochemical Incineration of Organic Pollutants on Boron-Doped Diamond Electrode. Evidence for Direct Electrochemical Oxidation Pathway. *J. Phys. Chem. B* **2003**, *107*, 13389–13395. [CrossRef]
129. Barisci, S.; Suri, R. Electrooxidation of short and long chain perfluorocarboxylic acids using boron doped diamond electrodes. *Chemosphere* **2020**, *243*, 125349. [CrossRef] [PubMed]
130. Guan, B.; Zhi, J.; Zhang, X.; Murakami, T.; Fujishima, A. Electrochemical route for fluorinated modification of boron-doped diamond surface with perfluorooctanoic acid. *Electrochem. Commun.* **2007**, *9*, 2817–2821. [CrossRef]
131. Zhao, G.; Zhang, Y.; Lei, Y.; Lv, B.; Gao, J.; Zhang, Y.; Li, D. Fabrication and Electrochemical Treatment Application of a Novel Lead Dioxide Anode with Superhydrophobic Surfaces, High Oxygen Evolution Potential, and Oxidation Capability. *Environ. Sci. Technol.* **2010**, *44*, 1754–1759. [CrossRef]
132. Zhuo, Q.; Xiang, Q.; Yi, H.; Zhang, Z.; Yang, B.; Cui, K.; Bing, X.; Xu, Z.; Liang, X.; Guo, Q.; et al. Electrochemical oxidation of PFOA in aqueous solution using highly hydrophobic modified PbO_2 electrodes. *J. Electroanal. Chem.* **2017**, *801*, 235–243. [CrossRef]
133. Aquino, J.M.; Rocha-Filho, R.C.; Ruotolo, L.A.M.; Bocchi, N.; Biaggio, S.R. Electrochemical degradation of a real textile wastewater using β-PbO_2 and DSA® anodes. *Chem. Eng. J.* **2014**, *251*, 138–145. [CrossRef]
134. Mukimin, A.; Vistanty, H.; Zen, N. Oxidation of textile wastewater using cylinder Ti/β-PbO_2 electrode in electrocatalytic tube reactor. *Chem. Eng. J.* **2015**, *259*, 430–437. [CrossRef]
135. Zhong, C.; Wei, K.; Han, W.; Wang, L.; Sun, X.; Li, J. Electrochemical degradation of tricyclazole in aqueous solution using Ti/SnO_2–Sb/PbO_2 anode. *J. Electroanal. Chem.* **2013**, *705*, 68–74. [CrossRef]
136. Song, S.; Fan, J.; He, Z.; Zhan, L.; Liu, Z.; Chen, J.; Xu, X. Electrochemical degradation of azo dye C.I. Reactive Red 195 by anodic oxidation on Ti/SnO_2–Sb/PbO_2 electrodes. *Electrochim. Acta* **2010**, *55*, 3606–3613. [CrossRef]
137. Yang, B.; Wang, J.; Jiang, C.; Li, J.; Yu, G.; Deng, S.; Lu, S.; Zhang, P.; Zhu, C.; Zhuo, Q. Electrochemical mineralization of perfluorooctane sulfonate by novel F and Sb co-doped Ti/SnO_2 electrode containing Sn-Sb interlayer. *Chem. Eng. J.* **2017**, *316*, 296–304. [CrossRef]
138. Xu, Z.; Yu, Y.; Liu, H.; Niu, J. Highly efficient and stable Zr-doped nanocrystalline PbO_2 electrode for mineralization of perfluorooctanoic acid in a sequential treatment system. *Sci. Total Environ.* **2017**, *579*, 1600–1607. [CrossRef] [PubMed]
139. Ellis, D.A.; Denkenberger, K.A.; Burrow, T.E.; Mabury, S.A. The Use of 19F NMR to Interpret the Structural Properties of Perfluorocarboxylate Acids: A Possible Correlation with Their Environmental Disposition. *J. Phys. Chem. A* **2004**, *108*, 10099–10106. [CrossRef]
140. Duan, X.; Wang, W.; Wang, Q.; Sui, X.; Li, N.; Chang, L. Electrocatalytic degradation of perfluoroocatane sulfonate (PFOS) on a 3D graphene-lead dioxide (3DG-PbO_2) composite anode: Electrode characterization, degradation mechanism and toxicity. *Chemosphere* **2020**, *260*, 127587. [CrossRef]
141. Shi, H.; Wang, Y.; Li, C.; Pierce, R.; Gao, S.; Huang, Q. Degradation of Perfluorooctanesulfonate by Reactive Electrochemical Membrane Composed of Magnéli Phase Titanium Suboxide. *Environ. Sci. Technol.* **2019**, *53*, 14528–14537. [CrossRef]
142. Huang, D.; Wang, K.; Niu, J.; Chu, C.; Weon, S.; Zhu, Q.; Lu, J.; Stavitski, E.; Kim, J.-H. Amorphous Pd-Loaded Ti4O7 Electrode for Direct Anodic Destruction of Perfluorooctanoic Acid. *Environ. Sci. Technol.* **2020**, *54*, 10954–10963. [CrossRef]
143. Wang, Q.; Liu, M.; Zhao, H.; Chen, Y.; Xiao, F.; Chu, W.; Zhao, G. Efficiently degradation of perfluorooctanoic acid in synergic electrochemical process combining cathodic electro-Fenton and anodic oxidation. *Chem. Eng. J.* **2019**, *378*, 122071. [CrossRef]

144. Abdelghafar, F.; Xu, X.; Jiang, S.P.; Shao, Z. Designing single-atom catalysts toward improved alkaline hydrogen evolution reaction. *Mater. Rep. Energy* **2022**, *2*, 100144. [CrossRef]
145. Zhuo, Q.; Li, X.; Yan, F.; Yang, B.; Deng, S.; Huang, J.; Yu, G. Electrochemical oxidation of 1H,1H,2H,2H-perfluorooctane sulfonic acid (6:2 FTS) on DSA electrode: Operating parameters and mechanism. *J. Environ. Sci.* **2014**, *26*, 1733–1739. [CrossRef]
146. Zhuo, Q.; Luo, M.; Guo, Q.; Yu, G.; Deng, S.; Xu, Z.; Yang, B.; Liang, X. Electrochemical Oxidation of Environmentally Persistent Perfluorooctane Sulfonate by a Novel Lead Dioxide Anode. *Electrochim. Acta* **2016**, *213*, 358–367. [CrossRef]
147. Lin, H.; Niu, J.; Liang, S.; Wang, C.; Wang, Y.; Jin, F.; Luo, Q.; Huang, Q. Development of macroporous Magnéli phase Ti_4O_7 ceramic materials: As an efficient anode for mineralization of poly- and perfluoroalkyl substances. *Chem. Eng. J.* **2018**, *354*, 1058–1067. [CrossRef]
148. Le, T.X.H.; Haflich, H.; Shah, A.D.; Chaplin, B.P. Energy-Efficient Electrochemical Oxidation of Perfluoroalkyl Substances Using a Ti_4O_7 Reactive Electrochemical Membrane Anode. *Environ. Sci. Technol. Lett.* **2019**, *6*, 504–510. [CrossRef]
149. Schaefer, C.E.; Andaya, C.; Urtiaga, A.; McKenzie, E.R.; Higgins, C.P. Electrochemical treatment of perfluorooctanoic acid (PFOA) and perfluorooctane sulfonic acid (PFOS) in groundwater impacted by aqueous film forming foams (AFFFs). *J. Hazard. Mater.* **2015**, *295*, 170–175. [CrossRef] [PubMed]
150. Chen, Y.; Guo, D.; Dong, X.; Li, Y.; Huang, Y.; Chen, H.; Li, S. Electrocatalytic degradation of perfluorooctanoic acid by LaNixY1-xO_3 (Y=Fe, Cu, Co, Sr) gas dispersion electrode. *J. Fluorine Chem.* **2021**, *242*, 109700. [CrossRef]
151. Zhang, Y.; Thomas, A.; Apul, O.; Venkatesan, A.K. Coexisting ions and long-chain per- and polyfluoroalkyl substances (PFAS) inhibit the adsorption of short-chain PFAS by granular activated carbon. *J. Hazard. Mater.* **2023**, *460*, 132378. [CrossRef]
152. Xiong, X.; Shang, Y.; Bai, L.; Luo, S.; Seviour, T.W.; Guo, Z.; Ottosen, L.D.M.; Wei, Z. Complete defluorination of perfluorooctanoic acid (PFOA) by ultrasonic pyrolysis towards zero fluoro-pollution. *Water Res.* **2023**, *235*, 119829. [CrossRef]